VON KARMAN INSTITUTE FOR FLUID DYNAMICS

LECTURE SERIES 1985-03

MEASUREMENT TECHNIQUES IN TURBOMACHINES

FEBRUARY 25 - MARCH 1, 1985

SHORT DURATION HEAT TRANSFER MEASUREMENTS

TONY ARTS & CENGIZ CAMCI - VKI

LIST OF SYMBOLS

A^*/β	calibration coefficient of the analog circuits
c	specific heat
C	capacitance
i	current
M	Mach number
p	pressure
$\dot{q}_s$	wall heat flux
Re	Reynolds number
R_∞	thin film gauge resistance
s	curvilinear coordinate
T	temperature
t	time
Tu	turbulence intensity
V_0	thin film reference voltage
ΔN	digitized raw heat transfer signal
$\Delta R/\Delta T$	thin film gauge resistance/temperature ratio
α_R	thin film temperature coefficient $\frac{1}{R_\infty}\frac{\Delta R}{\Delta T}$
α	thermal diffusivity $\left(\frac{k}{\rho c}\right)$
θ	temperature difference $(T(x) - T_\infty)$
ρ	density
$\sqrt{\rho c k}$	substrate thermal product

LIST OF FIGURES

1. INTRODUCTION

The most classical way to improve the thermal efficiency of a Joule/Brayton cycle is to increase the turbine entry temperature and pressure ratio. As a result, specific fuel consumption, size and weight of aero-engines were significantly reduced during the two last decades. A 25/1 pressure ratio and a 1800 K TET are typical values encountered in high performance jet engines (Ref. 1). However, the latter are limited by material properties and an efficient internal and/or external cooling is most often required to overcome the high temperature operation problems. An accurate knowledge of the convective heat flow across the blade surfaces and the endwalls is therefore an important, even essential part of their design, in order to perform any detailed heat conduction or thermal stress analysis.

From a numerical point of view, the accurate heat transfer pattern determination in a turbine, with or without any cooling scheme, remains an extremely difficult problem. The flow is highly three dimensional, viscous, rotational, transonic and unsteady and Reynolds numbers of the order of 5.10^5 ... 3.10^6 (based on the true chord and on the downstream conditions) are most often encountered. Also the free stream turbulence levels are quite high. In such an environment, the solution of the full three dimensional Navier-Stokes equations requires an enormous computational effort (numerical method, CPU time and computer memory) and will still remain a challenge for the next years. In order to help the designer, simplified approaches have been considered : boundary layer codes, two dimensional Navier-Stokes equations programs (parabolized or partially parabolized solutions) etc, (Refs. 2,3,4,5,6,7,8,9). These codes depend anyway on some empirical or experimental input (Reynolds stress modelling, boundary layer transition criterion, intermittency behaviour, etc).

The experimental techniques currently used to investigate heat transfer on gas turbine components can be divided into two categories : steady state techniques and short duration or transient techniques. The first approach has been intensively used in order to investigate the basic principles of convective heat transfer (e.g., Refs. 10,11,12,13,14). Their disadvantage is that, most often, they are not able to provide simultaneously the correct free stream Mach and Reynolds numbers, turbulence intensity and free stream/wall/coolant temperature ratios. Only engine test rigs provide a full similarity but their construction, maintenance and operating costs prohibit research in university or non industrial research laboratories. On the other hand, the advantage of short duration facilities is to run at full scale (mean) engine conditions but in a transient mode so that, although all the flow parameters are correctly duplicated, the total energy consumption is tremendously reduced. However, quite sophisticated test rigs, instrumentation and data acquisition capabilities are required.

2. SHORT DURATION TESTING FACILITIES

Three categories of short duration testing facilities are principally used to investigate heat transfer and aerodynamic phenomena in turbine components :

- shock tunnels
- blowdown cascades
- isentropic light piston compression tubes.

2.1 Shock tunnels

Most of the early heat transfer research performed in shock tubes was associated with hypersonic vehicle problems. High enthalpy and high Mach number flows were most often produced. The flow conditions in a turbine are, however, much less severe with respect to temperatures, pressures and velocities. It is, however, possible to operate a reflected shock tunnel in a subsonic mode to produce realistic (from a turbomachinery point of view) Mach and Reynolds numbers as well as free stream/wall/coolant temperature ratios (Ref. 15). This technique has been applied e.g. by Louis at M.I.T. (Refs. 16,17) on simplified gas turbine models (flat plate, channel) and by Dunn at Calspan (Refs. 18,19,20,21) on stationary full scale vanes and rotors. The facility used at Calspan is presented in figure 1.

2.2 Blowdown cascades

Short duration blowdown cascades were primarily used for aerodynamic studies; more and more heat transfer investigations are, however, also conducted. The facility used by Louis et al. at M.I.T. (Refs. 16,17) (Fig. 2) is composed of an air supply system (17 bar), a turbine auxiliary to accelerate the turbine to near test RPM before the main flow is introduced, a pebble bed heater allowing a maximum inlet temperature of 460°K for a maximum total pressure of 7 bar, a diaphragm section, a mass flow monitoring throat, a supersonic diffuser section and a subsonic diffuser. A short duration blowdown facility was developed at Oxford University (Ref. 22, Fig. 3) in order to simulate both free stream Reynolds and Mach numbers but has been used, up to now, only for aerodynamic measurements; the temperature ratios are not duplicated. The facility consists of a regulated air supply, a plenum chamber, the test section, tandem ejector pump (Ref. 23) and a detuner. A short duration blowdown turbine facility was also developed at M.I.T. by Epstein et al. (Refs. 24,25, Fig. 4). This facility is able to provide flows with 10 bar inlet pressure and 533 K turbine inlet temperature. It is primarily intended for the exploration of unsteady, three dimensional fluid mechanics and heat transfer in turbine stages. It is made of a supply tank, a fast acting inlet valve, the test section, a dump tank and an eddy current brake absorbing the power developed by the turbine.

2.3 Isentropic light piston compression tubes

The isentropic light piston compression tube facility was conceived in order to fulfil the need for a short duration wind tunnel which could produce free stream Mach and Reynolds numbers and gas/wall/coolant temperature ratios typically encountered in actual aero-engines; the development of this kind of facility is due to Schultz and Jones (Ref. 15,26,27). A similar facility was built at the von Karman Institute by Richards et al. (Ref. 28).

The facility is schematically described in figure 5. It is made of four main components : a high pressure air reservoir, the compression tube, the test section and the downstream dump tank. The operating principle consists in assigning to the free stream flow values of total pressure and temperature by means of an isentropic compression. This compression is obtained from a light piston sliding slowly, practically without friction inside the tube. The piston is driven by the air supplied by the high pressure reservoir. Once the given total pressure and temperature are reached, a fast operating valve (valve B) links the compression tube with the test section. By acting on the opening of valve A, always chocked, the velocity of the piston and hence the free stream aerodynamic properties can be kept constant between the opening time of valve B and the end of the stroke of the piston. The dump tank, hermetically isolated from atmosphere, allows an overall pressure level adjustment, providing an independent definition of free stream Mach and Reynolds numbers. The detailed thoery of the flow in a compression tube is given in reference 26.

The evolution in time of some typical flow variables is shown in figure 6 :

- tube pressure (a)
- free stream total pressure (b)
- wall heat flux rate (c)
- wall temperature (d)

The low frequency oscillation observed on these traces is due to the finite mass of the piston. As a matter of fact, when valve B opens, the velocity of the gas ahead of the piston suddenly rises, function of the tube/test section cross area ratio. Because of its finite mass, the piston cannot instantaneously adjust its velocity; the pressure ahead of the piston falls and it starts to oscillate. In order to avoid this phenomenon, either a compensation system, described in reference 27 has to be installed, or very light pistons (e.g., made of carbon fibre) must be used.

3. SHORT DURATION HEAT TRANSFER MEASUREMENT TECHNIQUES

The use of any short duration facility requires a fast response instrumentation. In these facilities, the model never attains an equilibrium temperature and it is the nature of its approach to such thermal equilibrium that enables the determination of the convective heat flux rate. The models are most often constructed from relatively simple low or high conductivity materials. The sudden establishment of the high temperature flow results in a fast rise of the surface temperature of the model; different transducers can be used to measure the temperature evolution in order to deduce the local heat flux rate. Three important measurement principles are (Ref. 29) :

- gauges whose operation is based on a semi-infinite model assumption (thin film thermometers);
- calorimeter gauges;
- optical measurement methods.

Among this non limitative list of techniques, the first one seems to be the most popular to be applied in turbomachinery heat transfer measurements. Therefore, it will be described in a detailed way. A short description of the two other approaches will also be given.

3.1 Thin film heat transfer gauges

A thin film heat transfer gauge is made of a thin strip of conducting material, e.g. platinum, mounted on a semi-infinite low conductivity substrate, e.g. quartz. It acts as a variable resistance thermometer : any variation in its temperature is measured by its variation in resistance; this implies that the film must be sufficiently thin to avoid any undesirable influence on the temperature evolution of the substrate.

3.1.1 Transient heat conduction in a semi-infinite body

The one dimensional differential equations describing heat conduction across a metallic thin film and the substrate on which it is deposited are written as follows (Fig. 7) :

$$\frac{\partial^2 \theta_1}{\partial x^2} = \frac{1}{\alpha_1} \frac{\partial \theta_1}{\partial t} \qquad (1a)$$

$$\theta(x,t) = T(x,t) - T(\infty)$$

$$T(x,t) \to T(\infty) \iff x \to \infty$$

$$\frac{\partial^2 \theta_2}{\partial x^2} = \frac{1}{\alpha_2} \frac{\partial \theta_2}{\partial t} \qquad (1b)$$

The subscripts 1 and 2 refer respectively to the thin film and the substrate; $\alpha \left(= \frac{k}{\rho c}\right)$ is the thermal diffusivity. The equations have to satisfy the following boundary conditions :

$$x = 0 \quad : \quad - k_1 \frac{\partial \theta_1}{\partial x} = \dot{q}_s \qquad (2a)$$

$$x = \varepsilon \quad : \quad k_1 \frac{\partial \theta_1}{\partial x} = k_1 \frac{\partial \theta_2}{\partial x} \qquad (\varepsilon = \text{thin film thickness}) \tag{2b}$$

$$\theta_1 = \theta_2$$

$$x = \infty \quad : \quad \theta_2 = 0 \tag{2c}$$

Equation (2c) expresses an important assumption, i.e., the substrate is considered to be semi-infinite. Furthermore, one assumes that conduction effects across the film are negligible and hence, that the film is at a uniform temperature because of its small thickness ε. If ε tends to 0, the system of equations (1) and the corresponding boundary conditions become :

$$\frac{\partial^2 \theta}{\partial x^2} = \frac{1}{\alpha} \frac{\partial \theta}{\partial t} \tag{3}$$

$$x = 0 \quad - k \frac{\partial \theta}{\partial x} = \dot{q}_s \tag{4a}$$

$$x = \infty \quad \theta = 0 \tag{4b}$$

The initial condition (t = 0) of this system is expressed as :

$$t = 0 \quad : \theta = 0 \tag{5}$$

The solution of equation (3) is obtained from the application of a Laplace transformation. A full derivation is presented in reference 30 and provides the following result, expressed as a surface temperature rise due to a time dependent surface heat flux rate variation :

$$\theta_s = \frac{1}{\sqrt{\rho c k}} \int_{\tau=0}^{t} \frac{\dot{q}_s(\tau)}{\sqrt{\pi (t-\tau)}} d\tau \tag{6}$$

The thermal product $\sqrt{\rho c k}$ is defined using the substrate material properties. If a constant heat flux is applied to the surface, a parabolic temperature rise will be observed. As a matter of fact, the integration of equation (6) provides the following result :

$$\theta_s = \frac{1}{\sqrt{\rho c k}} \frac{2 \dot{q}_s \sqrt{t}}{\sqrt{\pi}} \tag{7}$$

Alternatively, the wall heat flux is expressed as follows :

$$\dot{q}_s = \frac{\sqrt{\pi}}{2} \sqrt{\frac{\rho c k}{t}} \theta_s \tag{8}$$

The surface temperature θ_s can be calculated from the resistance variation of the thin film :

$$R = R_\infty \left[1 + \alpha_D (T - T_\infty)\right] \tag{9}$$

where R and R_∞ are the film resistances at temperatures T and T_∞ and α_R is the resistance temperature coefficient. If the film is supplied with constant current, equation (9) becomes

$$V = V_0 \left[1 + \alpha_R (T-T_\infty)\right]$$

and the surface temperature rise θ_s is expressed as follows :

$$\theta_s = T-T_\infty = \frac{V-V_0}{\alpha_R V_0} = \frac{\Delta V}{\alpha_R V_0}$$

V_0 is the film voltage at time t = 0. Substituting this last equation in (8), one gets the surface heat flux :

$$\dot{q}_s = \frac{\sqrt{\pi}}{2} \sqrt{\frac{\rho c k}{t}} \frac{\Delta V}{\alpha_R V_0} \qquad (9)$$

α_R is measured before each test and is equal to :

$$\alpha_R = \frac{1}{R_\infty} \frac{(R-R_\infty)}{(T-T_\infty)}$$

The determination of R_∞ might eventually be done at a calibration temperature T_{cal} different from T_∞. This effect is taken into account through a classical temperature correction and one gets finally :

$$\dot{q}_s = \frac{\sqrt{\pi}}{2} \sqrt{\frac{\rho c k}{t}} \frac{\Delta V}{V_0} \frac{R_{cal}}{\Delta R/\Delta T} \left[1 + \frac{1}{R_{cal}} \frac{\Delta R}{\Delta T} (T_\infty - T_{cal})\right] \qquad (10)$$

The procedure used to deposit the platinum thin film heat transfer gauges on their substrate is fully described in references 29, 30 and 31.

3.1.2 Electrical analogy of heat transfer into a semi-infinite body

Although an analytical solution of one dimensional transient heat conduction into a semi-infinite body is provided by equation (10), the wall heat flux measurements are most often performed using an electrical analogy. This approach results in a much faster and more precise quantitative determination of the time dependent wall heat flux from measured wall temperatures compared to its purely numerical evaluation.

An electrical analogy of a heat flow into a semi-infinite solid may be obtained from a series of resistances and capacitances in which voltages and currents behave similarly to temperatures and heat fluxes. The behaviour of these circuits may be explained by looking at the equations modelling both configurations (Fig. 8) :

The rate of gain of energy in an element Δx is :

$$-\frac{\partial \dot{q}}{\partial x}\Delta x \qquad (11a)$$

which, by conservation of energy, is equal to :

$$\rho c \Delta x \frac{\partial T}{\partial t} \qquad (12a)$$

and hence

$$\frac{\partial \dot{q}}{\partial x} = -\rho c \frac{\partial T}{\partial t} \qquad (13a)$$

The heat conduction equation is expressed as

$$\dot{q} = -k \frac{\partial T}{\partial t} \qquad (14a)$$

and combining with the preceding equation one gets :

$$\frac{\partial^2 T}{\partial x^2} = \frac{\rho c}{k} \frac{\partial T}{\partial t} \qquad (15a)$$

The rate of gain of charge in an element Δx is :

$$-\frac{\partial i}{\partial x}\Delta x \qquad (11b)$$

which, by conservation of charge is equal to :

$$c'\Delta x \frac{\partial V}{\partial t} \qquad (12b)$$

(r' and c' being the resistance and capacitance per unit length)

and hence

$$\frac{\partial i}{\partial x} = -c' \frac{\partial V}{\partial t} \qquad (13b)$$

Ohm's law is expressed as :

$$i = -\frac{1}{r'\Delta x}\frac{\partial V}{\partial x}\Delta x = -\frac{1}{r'}\frac{\partial V}{\partial x} \qquad (14b)$$

and combining with the preceding equation one gets :

$$\frac{\partial^2 V}{\partial x^2} = r'c'\frac{\partial V}{\partial t} \qquad (15b)$$

The last two equations show clearly the analogy existing between the heat diffusion equation and the electrical transmission line equation.

The initial and boundary conditions necessary to solve equation (15b) are :

$t = 0$: $V = 0$

$x = \infty$: $V = 0$

$x = 0$: $i_{in} = -\frac{1}{r'}\frac{\partial V}{\partial x}$

The solution of this partial differential equation is obtained from the application of a Laplace transformation. The following result is obtained (Ref. 30, Figs. 8-9) :

$$\dot{q}_s = \sqrt{\rho c k}\sqrt{\frac{r'}{c'}}\frac{1}{\alpha_R V_0}\frac{V_{OUT}}{R_1} \qquad (16)$$

This equation is combined with the heat flux expression obtained in the preceding section (10) to obtain :

$$\dot{q}_s = \frac{\sqrt{\pi}}{2}\sqrt{\frac{\rho c k}{t}}\frac{\Delta V}{\alpha_R V_0} = \sqrt{\rho c k}\sqrt{\frac{r'}{c'}}\frac{1}{\alpha_R V_0}\frac{V_{OUT}}{R_1} \qquad (17)$$

The characteristics of the analog circuit can be defined by a calibration coefficient :

$$\frac{A^*}{\beta} = \frac{\sqrt{\pi}}{2}\frac{1}{\sqrt{t}}\frac{\Delta V}{V_{out}} = \sqrt{\frac{r'}{c'}}\frac{1}{R_1} \qquad (18)$$

The wall heat flux is finally expressed by the following equation, taking into account a temperature correction on α_R :

$$\dot{q}_s = \frac{A^*}{\beta}\frac{\Delta V}{V_0}\frac{\sqrt{\rho c k}}{\alpha_R}\left[1 + \alpha_R (T_\infty - T_{cal})\right] \qquad (19)$$

The actual r' and c' values required in the analog circuits are difficult to define. Any arrangement of resistive and capacitive components represents a semi-infinite heat transfer provided that the product $\sqrt{r'c'}$ (analogous to $\sqrt{\rho c k}$) remains constant with time. The criteria by which different circuits may be evaluated are related to the speed and duration of their response to inputs, i.e., changes in heat flux. Two characteristic times have to be considered (Fig. 10) :

- the response time : it is the time required for the analog output to fully account for an alteration in the voltage input signal;
- the operation time : it is the time during which the output signal of the analog circuit represents a particular heat transfer profile with a given accuracy.

The aim in analog circuit design is to minimize the response time and to maximize the operation time. The T-section presented in figure 9 proved to have a short response time, equal to RC provided that all stages are made of identical components. The operation time, defined in figure 10, is calculated as $0.2\ n^2$ RC where n is the number of stages. When long testing times or high measurement accuracy are required, arithmetically increasing components are preferred (Ref. 30).

3.1.3 Details of the assumptions

In the preceeding section, three important assumptions were made :

- the heat transfer is considered to be one dimensional;
- the substrate has a semi-infinite behaviour;
- the film is very thin.

Each of these has to be satisfied if a correct measurement of the wall heat flux using the present technique is desired.

3.1.3.1 One dimensional heat transfer

The heat transfer into the substrate must be one dimensional. Most of the time, this assumption is verified if the gauges are not located near the edges of the model or near holes (e.g., film cooling holes) in the substrate. A good empirical rule is to deposit the gauges away from the substrate discontinuities at a distance at least equivalent to that required for a semi-infinite behaviour (§ 3.1.3.2).

3.1.3.2 Substrate thickness

The substrates on which the thin film gauges are deposited must be thick enough so that the heat transfer across them is similar to the one into a semi-infinite solid. At the end of the test, θ_x/θ_s should be negligible at the base of the substrate. Ideally, $\theta_x (= T-T_\infty)$ should be equal to 0. A quantitative solution is found by using the heat flux/temperature equation, if a step-like variation is applied to the heat flux, one gets (Ref. 29) :

$$\frac{\theta_x}{\theta_s} = e^{-(x^*)^2} - \sqrt{\pi}\, x^*\, \mathrm{erfc}\,(x^*) \qquad (20)$$

$$x^* = \frac{x}{\sqrt{4\alpha t}}$$

Equation (20) is plotted in figure 11. It has been redrawn in a more explicit form for several insulating materials and several testing times in figure 12.

3.1.3.3 Thin film gauge thickness

The thin film gauges must not disturb the surface heat flux. This is generally verified because of their minimal thickness (10^{-6} ... 10^{-7} m) and their high thermal conductivity. It can be shown (Ref. 29) that the ratio of the heat flux through the film to the actual one felt by the substrate is given by the following expression :

$$\frac{\dot{q}}{\dot{q}_0} = 2a\,\frac{\alpha_1 t}{\varepsilon}\left[\frac{1}{\sqrt{\pi}} - \frac{2a}{1+a}\sum_{n=0}^{\infty}\left(\frac{1-a}{1+a}\right)^n \cdot i \cdot \mathrm{erfc}\left[\frac{\frac{n+1}{2}}{\frac{\sqrt{\alpha_1 t}}{\varepsilon}}\right]\right] \qquad (21)$$

$$a = \sqrt{\frac{\rho_2 c_2 k_2}{\rho_1 c_1 k_1}} \qquad \begin{cases} 1 : \text{thin film} \\ 2 : \text{substrate} \end{cases}$$

$$i^2 = -1$$

ε = thin film thickness

Equation (21) is plotted in figure 13; it has been redrawn in figure 14 to compare the response times of platinum thin films being respectively 1 and 2 µm thick.

3.1.4 Measurement procedure - data reduction

The evaluation of the local wall heat flux is performed using equation (19), applied for each thin film. The present measurement technique first requires a calibration of all analog circuits providing the temperature/heat flux conversion, in order to obtain their gain, i.e., the A^*/β coefficient. This calibration is obtained by applying a parabolic voltage variation at the input of the analog circuits. The value of each reference voltage V_0, applied to the thin films, is measured before each test and, additionally, provides a correct evaluation of the initial wall temperature T_∞. The substrate thermal product $\sqrt{\rho ck}$ is determined by a comparative measurement from gauges mounted on several substrates and quartz (which is a well defined substrate) in an impingement flow situation. The ratio $(\Delta R/\Delta T)$ is determined for each film from a preliminary resistance versus temperature calibration, performed in a temperature controlled oil bath; a typical evaluation is presented in figure 15. The resistance R_{cal} of each gauge is measured at a given temperature T_{cal} and corrected for the corresponding initial wall temperature T_∞. The raw signal ΔV acquired by the computer, consists of a series of integer values.

Solving equation (19) provides the wall heat flux time history of each of the platinum thin films during a test. The temperature time history is then numerically obtained from the following equation (Ref. 32) :

$$T(t) = \frac{4}{3\sqrt{\rho ck\pi}} \sum_n \left[\left(\frac{\dot{q}_{n+1} - 2\dot{q}_n + \dot{q}_{n-1}}{\Delta\tau} \right) (t-t_n)^{3/2} \, H\,(t-t_n) \right] \qquad (22)$$

where $\dot{q}_n$ is the measured heat flux at time $t_n = n\Delta\tau$ and $H(t-t_n)$ is equal to 1 for $t \geq t_n$ and to 0 for $t < t_n$. A combination of both wall heat flux and temperature data provides a heat flux versus temperature relation for each thin film and each test. This curve is then extrapolated to isothermal wall conditions, i.e., zero surface temperature rise in order to obtain a heat transfer coefficient (Fig. 16).

3.1.5 Uncertainty analysis

Wall heat fluxes are computed using equation (19) :

$$\dot{q}_s = \frac{A^*}{\beta} \frac{N_{out}}{V_0} \frac{\sqrt{\rho ck}}{\alpha_R} \left[1 + \alpha_R (T_\infty - T_{cal}) \right] \qquad (23)$$

where N_{out} is the digitized analog circuit output, proportional to V_{OUT}. The uncertainty on wall heat flux is evaluated as follows (Ref. 33) :

$$\delta\dot{q}_s = \left[\left(\frac{\partial \dot{q}_s}{\partial \left(\frac{A^*}{\beta} \right)} \delta \frac{A^*}{\beta} \right)^2 + \left(\frac{\partial \dot{q}_s}{\partial N_{OUT}} \delta N_{OUT} \right)^2 + \left(\frac{\partial \dot{q}_s}{\partial V_0} \delta V_0 \right)^2 + \left(\frac{\partial \dot{q}_s}{\partial (\sqrt{\rho ck})} \delta (\sqrt{\rho ck}) \right)^2 + \left(\frac{\partial \dot{q}_s}{\partial \alpha_R} \delta \alpha_R \right)^2 \right]^{1/2} \qquad (24)$$

where :

$$\frac{\partial \dot{q}_s}{\partial \frac{A^*}{\beta}} = \frac{N_{OUT}}{V_0} \frac{\sqrt{\rho c k}}{\alpha_R}$$

$$\frac{\partial \dot{q}_s}{\partial N_{OUT}} = \frac{A^*}{\beta} \frac{1}{V_0} \frac{\sqrt{\rho c k}}{\alpha_R}$$

$$\frac{\partial \dot{q}_s}{\partial V_0} = \frac{A^*}{\beta} \frac{N_{OUT}}{\alpha_R} \sqrt{\rho c k} \left(- \frac{1}{V_0^2} \right)$$

$$\frac{\partial \dot{q}_s}{\partial (\sqrt{\rho c k})} = \frac{A^*}{\beta} \frac{N_{OUT}}{V_0} \frac{1}{\alpha_R}$$

$$\frac{\partial \dot{q}_s}{\partial \alpha_R} = - \frac{A^*}{\beta} \frac{N_{OUT}}{V_0} \frac{\sqrt{\rho c k}}{\alpha_R^2}$$

The estimated uncertainties on the different measurements, based on a 95% confidence level, are estimated as follows :

$\delta V_0 = \pm 0.005$ V

$\delta \alpha_R = \pm 4\ 10^{-5}$ 1/K

$\delta N_{OUT} = \pm 10$ data units

$\delta \frac{A^*}{\beta} = \pm 2.5\ 10^{-6}$ V/data units $\sqrt{\text{sec}}$

$\delta \sqrt{\rho c k} = 7\ 10^{3} \frac{W}{cm^2} \frac{\sqrt{\text{sec}}}{K}$

By substituting these values in equation (19), a wall heat flux uncertainty $\frac{\delta \dot{q}_s}{\dot{q}_s}$ of ± 7.5% has been determined. It should be noted that the main uncertainty contributions are due to the α_R and $\sqrt{\rho c k}$ terms.

3.2 Calorimeter gauges

All calorimeter gauges attempt to determine the instantaneous heat transfer rate to a surface by measuring the time rate of change of the thermal energy within an element of the surface. This element is usually in the form of a thin skin (2 ... 20 µm). The thermal energy is determined from a temperature measurement in or on the surfaces of this skin and it is the rate of change of this temperature that gives the heat flux into the exposed surface. Assuming there is no heat lost from the rear surface, the heat transfer rate per unit area is expressed as follows (Ref. 29) :

$$\dot{q}_s = \int_0^{\ell} \rho c \frac{\partial T}{\partial t} dt$$

or for constant ρ and c

$$\dot{q}_s = \rho c \ell \frac{dT_{mean}}{dt}$$

ρ and c are the density and specific heat of the calorimetric material whereas ℓ is its thickness. T is the temperature at a position within the surface.

Several calorimetric designs can be used (Ref. 29) :

- calorimeters without substrate
- calorimeters with substrate
- the Rose calorimeter gauge
- thin skin calorimeter models
- capsule calorimeter gauges
- thick wall calorimeters
- total calorimeters.

This technique has mainly been used for heat transfer measurements in hypersonic short duration facilities rather than in turbomachinery application. A full description is given in reference 29.

3.3 Optical methods

Optical methods are based on the visual effects produced by temperature changes. Under transient heating conditions, the surface temperature of a model increases and the temperature is determined by the dependence of radiation, either reflected or emitted by the surface, on the body temperature. The model is most often covered with special thermal sensitive paints which enhance this reflection or emission processes. These paints are widely used in the aero-engine industry, either to locate "hot spots" in combustion chambers or on blades, or to verify the improvement provided by the internal or external cooling scheme of any component. This technique provides a valuable overall view of the temperature and hence heat flux rate distribution before going to more sophisticated and more accurately instrumented models.

The surface temperature distribution can be provided by using (Ref. 29) :

- temperature sensitive colour-change paints
- phase change coatings
- liquid crystals (often used for transitional flows)
- thermographic phosphors (illuminated by ultra-violet light)
- infra red emission (infra red camera).

4. EXPERIMENTAL RESULTS

Experimental investigations are generally conducted on models presenting a similar configuration to real gas turbine elements. However, the analysis of individual effects such as free stream pressure gradient, wall curvature and roughness, degree of turbulence, secondary flows, geometry and spacing of film cooling holes, blowing ratio, density ratio, etc, is most often performed on simple models, e.g. flat or curved plates, without or with pressure gradients. Three applications will shortly be described in the next paragraph :

- convective heat transfer on a flat plate, with and without film cooling
- convective heat transfer on a high pressure rotor blade without film cooling
- convective heat transfer on a high pressure rotor blade with film cooling.

All these measurement results were obtained in the von Karman Institute isentropic light piston compression tube facility.

4.1 The VKI isentropic compression tube facility

The von Karman Institute isentropic compression tube facility (Fig. 17), constructed in 1978, consists of 5 m long, 1 m diameter cylinder containing a light weight piston, driven by the air of a high pressure reservoir. The piston is presently made of aluminium, has a honeycomb structure and weighs about 27 kg. The cylinder is isolated from the test section by a fast opening slide valve. As the piston moves, the gas in front of it is nearly isentropically compressed until it reaches the pressure, and hence temperature, levels defined by the operator. The fast opening valve is then actuated by means of a detonator, allowing the pressurized air to flow through the test section. Constant free stream conditions as well as heat flow rate are applied to the model until the piston completes its stroke. The complete opening of the shutter takes about 10 to 25 ms. The maximum test section dimensions are 250 × 100 mm^2. The free stream thermodynamic conditions can be varied between 300 and 600 K and 0.5 and 7 bar. A 5 m^3 dump tank allows downstream pressure adjustments between 0.1 and 4 bar. A typical test duration is about 400 ... 500 ms. Further details about this facility are described in references 28 and 34.

All the pressure, temperature and heat flux measurements are directly acquired by a DIGITAL PDP 11/34 computer by means of a high speed data acquisition system (Fig. 18). This unit, designed and built at the VKI, is characterized by three separate sections. The first one consists of 48 analog circuits, which provide the transformation of the heat flux gauge signals, proportional to the surface temperature, into signals proportional to the surface heat flux. The second section is composed of a series of 48 amplifiers and "low pass" filters. The last section consists of three analog to digital converters, a multiplexer and a buffer. The signals are digitized using 12 bit words. This data acquisition system can operate on 48 channels, with a maximum sampling frequency as high as 500 kHz.

4.2 Convective heat transfer on a flat plate, without and with film cooling

4.2.1 Model description

The model consists of an aluminium flat plate equipped with 18 platinum thin film gages deposited onto a quartz substrate (Fig. 19). The coolant is ejected through two

staggered rows of cylindrical holes, inclined at 35° with respect to the wall in the streamwise direction. The test section is equipped with a slot to bleed the lower wall boundary layer and to create a new boundary layer at the leading edge of the plate. The laminar to turbulent transition is induced artificially by means of a tripping wire : convective heat transfer across a turbulent boundary layer was only considered.

4.2.2 Results without coolant ejection

A first experiment was performed without any coolant ejection. During the test, free stream total pressure, total temperature and Mach number were kept constant at, respectively, 0.29 M Pa, 400 K and 0.6. The results are presented under the form of a Stanton number evolution plotted as a function of local Reynolds numbers (Fig. 20a) and are compared with the analytical solution obtained from a finite difference boundary layer code (STAN5) (Ref. 8) and from a classical correlation (Ref. 35). This quite academic application provides an idea about the accuracy of the measurement technique.

4.2.3 Results with coolant ejection

The effect of coolant flow ejection can be investigated through several parameters : blowing ratio, density ratio, velocity ratio, momentum ratio, etc. A typical example of the result is shown in figure 20b : the blowing rate is kept constant whereas the coolant temperature ratio is gradually decreased. This result has to be compared with those obtained by Metzger (Ref. 10) and demonstrates the importance of density effects in film cooling heat transfer.

4.3 Convective heat transfer on a high pressure rotor blade without film cooling

4.3.1 Model description

The measurements were carried out on a high pressure rotor blade profile designed at Rolls-Royce Ltd (Ref. 36). The blade profile is presented in figure 22 and the main cascade dimensions are summarized as follows :

blade height	100 mm
chord	69.84 mm
pitch	59.84 mm
inlet angle	40°0 (from the axial direction).

The blade instrumented for heat transfer measurements (Fig. 23) was milled from low conductivity "Macor" glass ceramic and 40 platinum thin film gauges were painted on its surface. The free stream turbulence was generated by a grid of circular bars oriented in the spanwise direction; its level was varied by displacing the grid upstream of the model.

The velocity distributions around the blade were obtained from local static pressure measurements, also performed in the isentropic compression tube facility. The latter were referred to the measured inlet total pressure in order to define an isentropic Mach number distribution (Fig. 24).

The heat transfer measurement results have been plotted under the form of a heat transfer coefficient (h) evolution as a function of a curvilinear coordinate (s) measured along the profile surface. In the present contribution, the heat transfer coefficient is defined as the ratio of the measured wall heat flux to the mainstream total-wall temperature difference

$$h = \frac{\dot{q}_w}{T_{0\infty} - T_w}$$

The total temperature was chosen equal to 420 K and the model was at room temperature before the test.

4.3.2 Measurement results

A typical result, demonstrating the effect of free stream turbulence intensity on heat transfer is presented in figures 25a,b. In the stagnation area, the heat flux level increases with free stream turbulence, as demonstrated by several authors (e.g., Ref. 37). Along the suction side, the laminar heating also increases, but less significantly, with the turbulence intensity, in accordance with other observations on the flow submitted to a pressure gradient along a curved surface (Ref. 34). When the free stream turbulence is increased from 1% to 8%, the transition onset moves upstream, towards the leading edge. Finally, a turbulent boundary layer develops until the trailing edge. Along the pressure side, the exact boundary layer state is difficult to define : destabilization of the boundary layer is expected because of concave curvature whereas the important favourable pressure gradient measured along the rear part of this surface (Fig. 24) would rather have a stabilizing effect. The flow is most probably transitional over the entire length of the pressure side. This idea is supported by looking at the effect that free stream turbulence has on the heat transfer distribution : a fully established turbulent boundary layer would not be affected at all.

As suggested in reference 38, it is also possible to determine the onset of transition by looking at the time history of the wall heat flux signals. Along the suction side, a typical example is presented in figure 26 ($Re_2 = 10^6$, $M_2 = 0.9$, $Tu = 4\%$). A typical laminar trace is first shown at s = 33 mm. The transition onset seems to take place at s = 43 ... 49 mm; some agitation, corresponding to turbulent spikes, is observed on these traces. This agitation becomes larger and larger for s = 55 ... 60 ... 67 mm and it looks like a turbulent boundary layer is established around s = 85 ... 90 mm. As a matter of fact, the heat transfer signals acquisition frequency was 1 kHz and they were filtered at 800 Hz; higher frequency phenomena present in the turbulent boundary layer could therefore obviously not be detected. Along the pressure side, no definite conclusions could be drawn. The boundary layer is most probably transitional rather than laminar or turbulent over the entire surface; therefore, no typical differences were observed on the heat flux traces.

4.4 Convective heat transfer on a high pressure rotor blade with film cooling

4.4.1 Model description

The measurements were carried out on the same rotor blade section as tested by Consigny and Richards (Ref. 34). The cascade geometry is summarized in figure 27. The blade

films were painted on its surface (Fig. 28). Three rows of cooling holes d = 0.8 mm, s/c = -0.01, 0. 0.01) are located around the leading edge (rows LP, LM, LS) and are spanwise angled at 30° from the tangential direction. Two staggered rows of shaped holes are located on the suction side (d = 0.8 mm, s/c = 0.20) and one row of shaped holes is located on the pressure side (d = 0.8 mm, s/c = 0.33). Three separate cavities are drilled along the blade height; they act as independent coolant plenum chambers. The coolant flow was supplied by a regenerative type cryogenic heat exchanger allowing a correct simulation of the coolant to free stream temperature ratio (Fig. 29). Pressure tappings and miniature thermocouples provide continuously the coolant characteristics at the three plenums inlet and outlet.

4.4.2 Measurement results

Two typical conclusions drawn from this experimental program (Refs. 31,39,40,41) are summarized as follows :

- along the suction side, laminar to turbulent transition is strongly influenced by the presence of the leading edge cooling holes, even when no coolant flow is ejected. This is demonstrated in figure 30 by comparing the present measurements with those performed on the identical but smooth profile by Consigny and Richards (Ref. 34). Along the pressure side, the boundary layer behaviour is dominated by the free stream pressure gradient rather than by the existence of the cooling holes

- significant coolant temperature effects are also observed. At low blowing rate (m = 0.40) (Fig. 31a), this effect is mainly observed up to 35 ... 40 hole diameters downstream of the suction side ejection rows when the coolant temperature is lowered from wall temperature to half of the mainstream level. However, at high blowing rate, the influence of the coolant temperature is felt much further downstream (Fig. 31b).

REFERENCES

1. OLSSON, U.: Advanced engine technology and its influence on aircraft performance.
AIAA Journal of Aircraft, Vol. 19, No. 5, May 1982, pp 380-384.

2. DODGE, P.: A numerical method for two and three dimensional viscous flow.
AIAA Paper 76-425.

3. LUCKING, P.: Numerische Berechnung des dreidimensionalen Reibungsfreien und Reibungsbehafteten Strömung durch Turbomaschinen.
Ph.D. Thesis, Aachen, 1982.

4. LAWERENZ, M.: Calculation of the three dimensional viscous flow in annular cascades using parabolized Navier-Stokes equations. In
"Secondary Flows and Endwall Boundary Layers in Axial Turbomachines",
VKI LS 1984-05.

5. MOORE, J. & MOORE, J.G.: Calculations of the three dimensional viscous flow and wake developemnt in a centrifugal impeller.
ASME Trans., Series A : J. Engineering for Power, Vol. 103, No. 2, April 1981,
pp 367-372.

6. MOORE, J. & MOORE, J.G.: Calculation of the horseshoe vortex flow without numerical mixing.
ASME Paper 84-GT-241.

7. HAH, C.: A Navier-Stokes analysis of three dimensional turbulent flows inside turbine blade rows at design and off-design conditions.
ASME Trans., Series A : J. Engineering for Gas Turbines and Power, Vol. 106, No. 2,
April 1984, pp 421-429.

8. CRAWFORD, M.E. & KAYS, W.M.: STAN5 - A program for numerical computation of two-dimensional internal/external boundary layer flows.
NASA CR 2742, 1976.

9. CRAWFORD, M.E.; KAYS, W.M.; MOFFAT, R.J.: Full coverage film cooling on flat plate, isothermal surfaces : a summary report on data and predictions.
NASA CR 3219, 1980.

10. METZGER, D.E.; CARPER, H.J.; SWANK, L.R.: Heat transfer with film cooling near nontangential injection slots.
ASME Trans., Series A : J. Engineering for Power, Vol. 90, No. 2, April 1968,
pp 157-163.

11. GOLDSTEIN, R.J.: Film cooling. In
"Advances in Heat Transfer", Vol. 7, pp 321-379.
New York, Academic Press, 1971.

12. GOLDSTEIN, R.J.; ECKERT, E.; RAMSEY, J.: Film cooling with injection through holes : adiabatic wall temperatures downstream of a circular hole.
ASME Trans., Series A : J. Engineering for Power, Vol. 90, No. 4, October 1968,
pp 384-395.

13. HAY, N.; LAMPARD, D.; SALYE, C.L.: Effects of the condition of the approach boundary layer and of mainstream pressure gradients on the heat transfer coefficient on film cooled surfaces.
ASME P 84-GT-47.

14. CRAWFORD, M.E.; CHOE, H.; KAYS, W.M.; MOFFAT, R.J.: Full-coverage film cooling heat transfer study - summary of data for normal hole injection and 30° slant-hole injection.
NASA CR 2648, March 1976.

15. JONES, T.V. & SCHULTZ, D.L.: A study of film cooling related to gas turbines using transient techniques.
ARC 32420, 1970.

16. LOUIS, J.F. et al.: Short duration studies of gas turbine heat transfer and film cooling effectiveness.
ASME Paper 74-GT-131.

17. LOUIS, J.F.: Systematic studies of heat transfer and film cooling effectiveness. In: "High Temperature Problems in Gas Turbine Engines" AGARD CP 229, 1977, paper 28.

18. DUNN, M.G. & STODDARD, F.J.: Application of shock tube technology to the measurement of heat transfer rate to gas turbine components. 11th International Symposium on Shock Tubes and Waves, July 1977.

19. DUNN, M.G. & STODDARD, F.J.: Measurement of heat transfer rate to a gas turbine stator. ASME Trans., Series A : J. Engineering for Power, Vol. 101, No. 2, April 1979, pp 275-280.

20. DUNN, M.G. & HAUSE, A.: Measurement of heat flux and pressure in a turbine stage. ASME Trans., Series A : J. Engineering for Power, Vol. 104, No. 1, January 1982, pp

21. DUNN, M.G.: Turbine heat flux measurements : influence of slot injection on vane trailing edge heat transfer and influence of rotor on vane heat transfer. ASME Paper 84-GT-175.

22. BAINES, N.C.; OLDFIELD, M.L.G.; JONES, T.V.; SCHULTZ, D.L.; KING; P.I.; DANIELS, L.C.: A short duration blowdown tunnel for aerodynamic studies on gas turbine blading. ASME Paper 82-GT-312.

23. BAINES, N.C.; OLDFIELD, M.L.G.; KING, P.I.; DANIELS, L.C.: The use of tandem ejector pumps in an intermittent blowdown tunnel. ASME Paper 84-GT-226.

24. EPSTEIN, A.H. & GUENETTE, G.R.: The M.I.T. blowdown facility. ASME Paper 84-GT-116.

25. EPSTEIN, A.H.: High frequency response measurements in turbomachinery. In "Measurement Techniques in Turbomachinery", VKI LS 1985-03, February 1985.

26. JONES, T.V.; SCHULTZ, D.L.; HENDLEY, A.D.: On the flow in an isentropic light piston tunnel. ARC R&M 3731, 1973.

27. SCHULTZ, D.L.; JONES, T.V.; OLDFIELD, M.L.G.; DANIELS, L.C.: A new transient cascade facility for the measurement of heat transfer rates. In: "High Temperature Problems in Gas Turbine Engines", AGARD CP 229, 1977, paper 31.

28. RICHARDS, B.E.: Heat transfer measurements related to hot turbine components in the von Karman Institute hot cascade tunnel. In: "Testing and Measurement Techniques in Heat Transfer and Combustion", AGARD CP 281, 1980, paper 6.

29. SCHULTZ, D.L. & JONES, T.V.: Heat transfer measurements in short duration hypersonic facilities. AGARDograph 165, February 1973.

30. LIGRANI, P.M.; CAMCI, C.; GRADY, M.S.: Thin film heat transfer gauge construction and measurement details. VKI TM 33, November 1982.

31. CAMCI, C.: An experimental and theoretical heat transfer investigation of film cooling on a high pressure gas turbine blade. Ph.D. Thesis (to be published).

32. OLDFIELD, M.L.G.; JONES, T.V.; SCHULTZ, D.L.: On-line computer for transient turbine cascade instrumentation. Trans. IEEE, Vol. AES-14, No. 5, September 1978.

33. KLINE, S.J. & McCLINTOCK, F.A.: Describing uncertainties in single sample experiments. Journal of Mechanical Engineering, Vol. 75, No. 1, January 1953, pp 3-8.

34. CONSIGNY, H. & RICHARDS, B.E.: Short duration measurements of heat transfer rate to a gas turbine rotor blade. ASME Trans., Series A : J. Engineering for Power, Vol. 104, No. 3, July 1982, pp 542-551.

35. KAYS, W.M. & CRAWFORD, M.E.: Convective heat and mass transfer.
New York, McGraw-Hill Book Co., 1980.

36. ARTS, T. & GRAHAM, C.G.: External heat transfer study on a high pressure turbine rotor blade.
Paper to be presented at the AGARD PEP 65th Symposium on Heat Transfer and Cooling in Gas Turbines, Bergen, Norway, May 6-10, 1985; also VKI Preprint 1985-12.

37. SMITH, M.C. & KUETHE, A.M.: Effects of turbulence on laminar skin friction and heat transfer.
The Physics of Fluids, Vol. 9, No. 12, December 1966, p 2337.

38. OLDFIELD, M.L.G.; KIOCK, R.; HOLMES, A.T.; GRAHAM, C.G..: Boundary layer studies on highly loaded cascades using heated thin films and a traversing probe.
ASME Trans., Series A : J. Engineering for Power, Vol. 103, No. 1, January 1981, pp 237-246.

39. CAMCI, C. & ARTS, T.: Experimental heat transfer investigation around the leading edge of a high pressure gas turbine rotor blade.
Paper to be presented at the 30th ASME Gas Turbine Conference, Houston, March 1985
VKI Preprint 1984-32. (ASME Paper 85 GT 114)

40. CAMCI, C. & ARTS, T.: Short duration measurements and numerical simulation of heat transfer along the suction side of a film cooled gas turbine blade.
Paper to be presented at the 30th ASME Gas Turbine Conference, Houston, March 1985,
VKI Preprint 1984-33. (ASME Paper 85 GT 111)

41. CAMCI, C. & ARTS, T.: Experimental convective heat transfer investigation around a film cooled high pressure turbine blade.
Paper to be presented at the ISABE Conference, China, 1985.

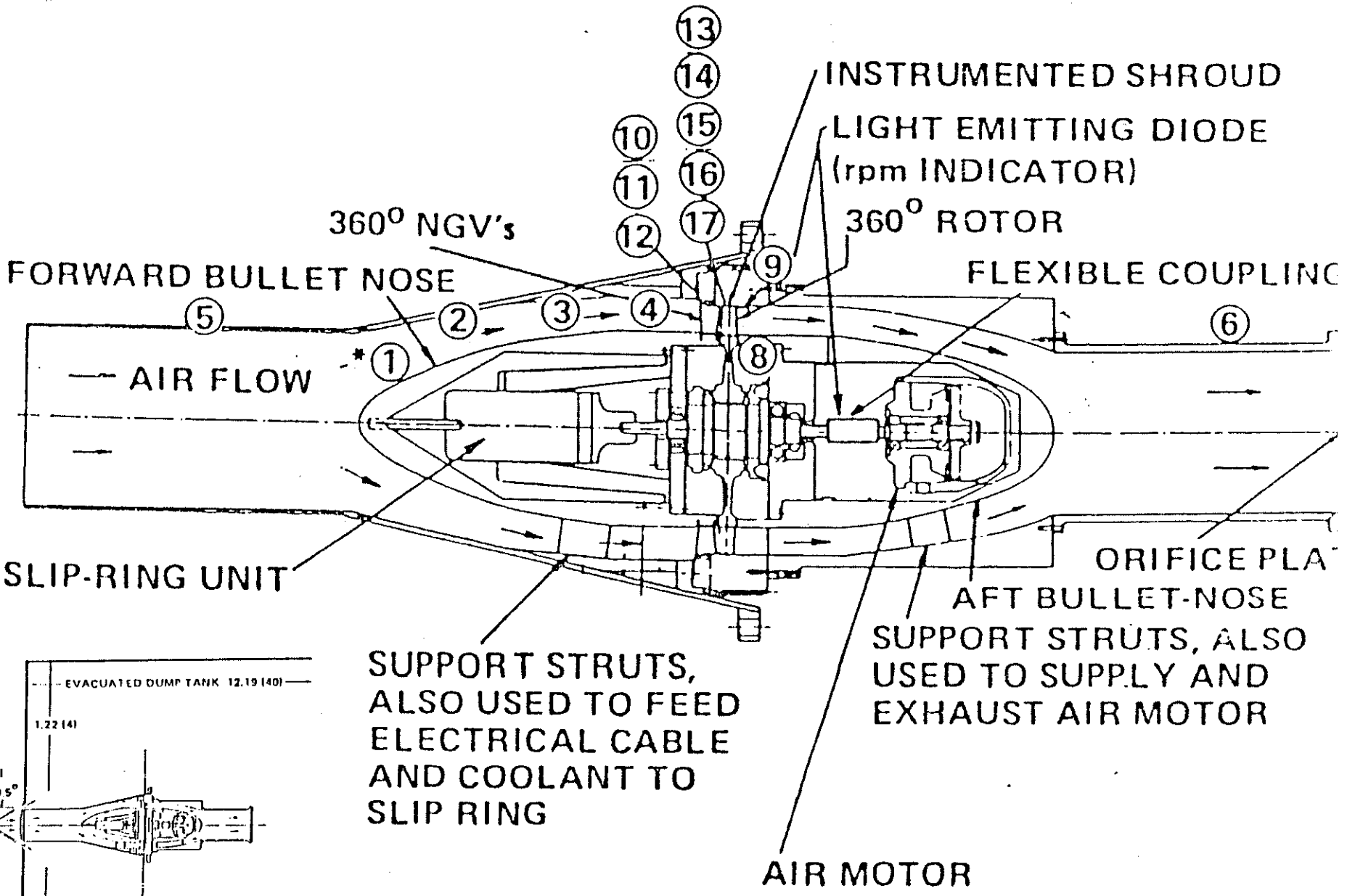

1. SHOCK TUBE USED BY DUNN AT CALSPAN (Ref. 20)

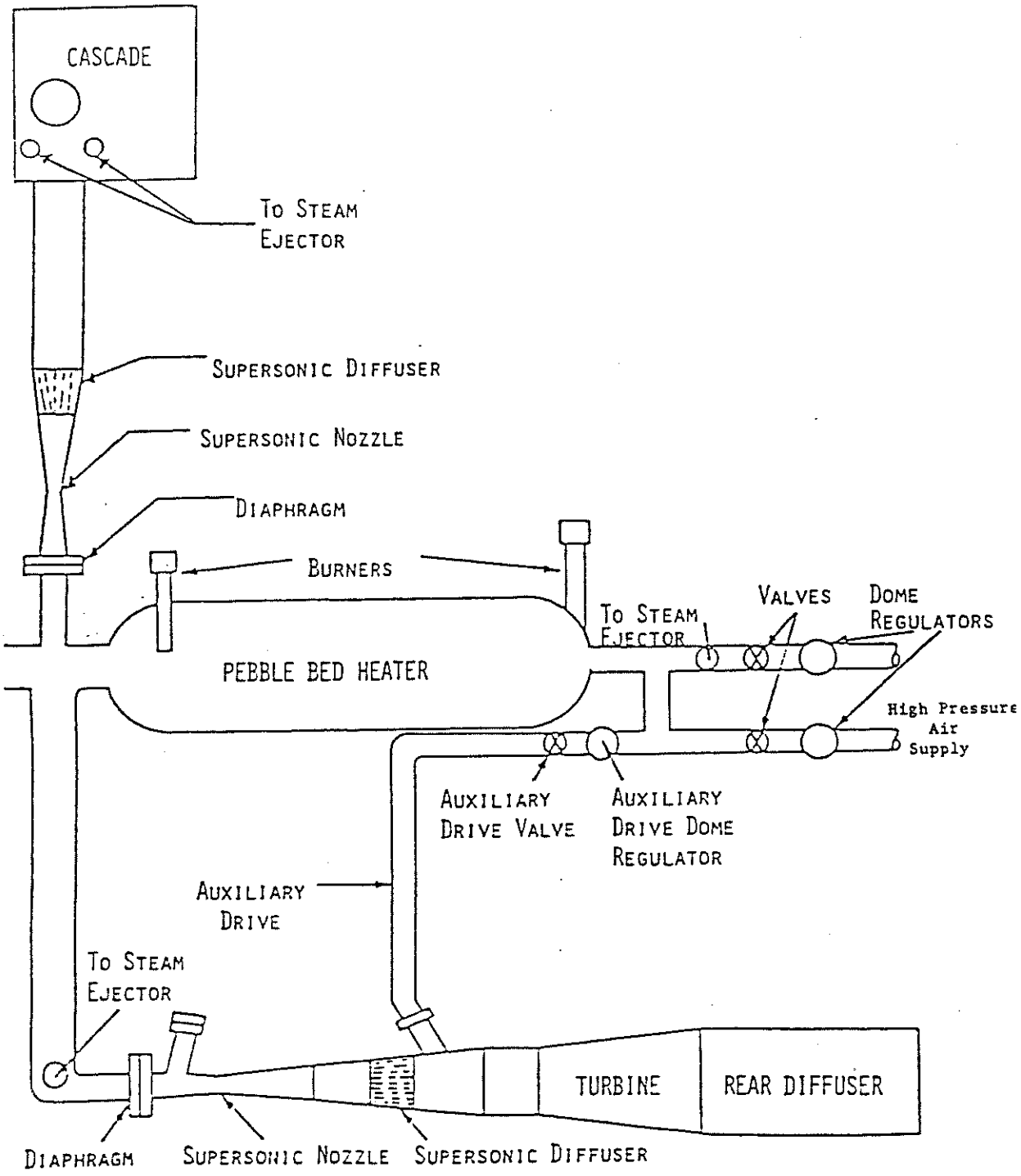

2. BLOWDOWN CASCADE FACILITY USED BY LOUIS AT MIT (Ref. 17)

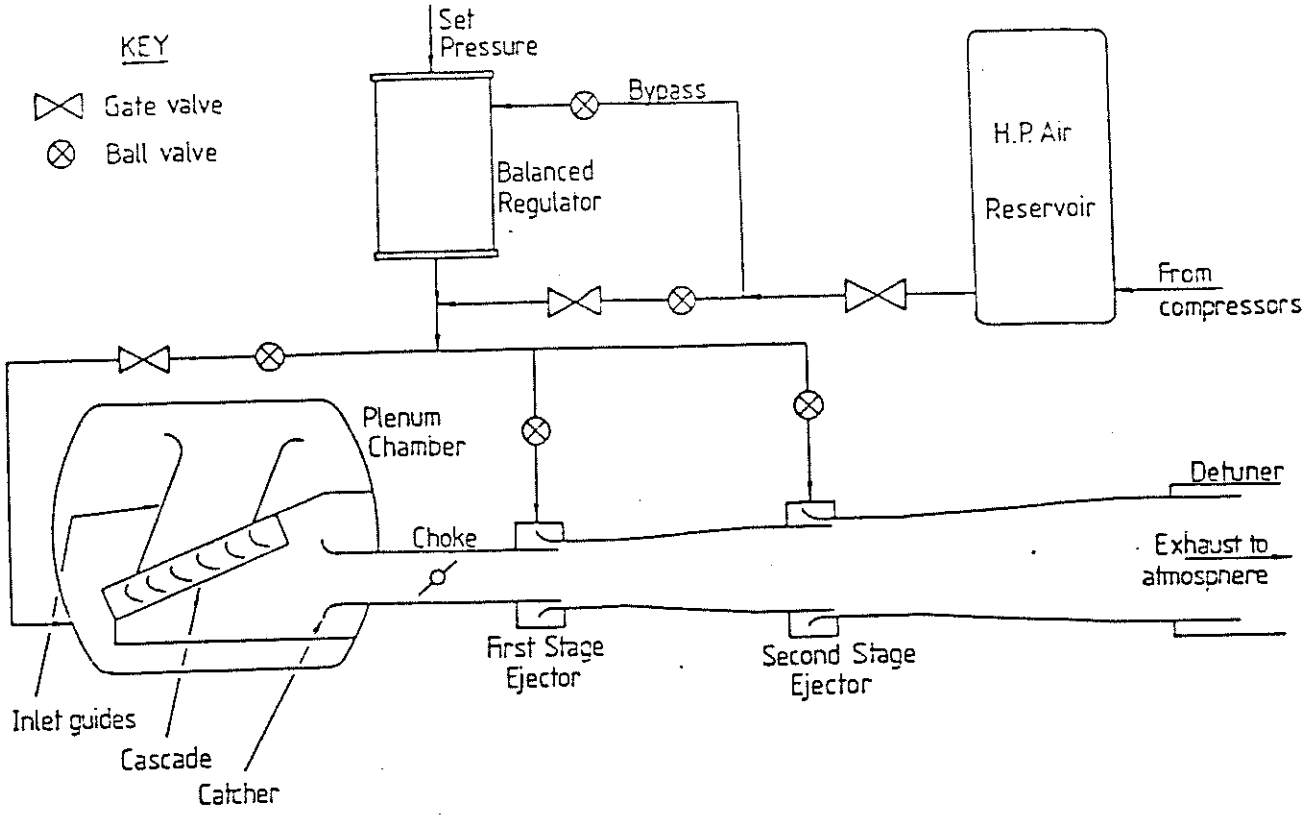

3. BLOWDOWN CASCADE FACILITY OF OXFORD UNIVERSITY
(Ref. 22)

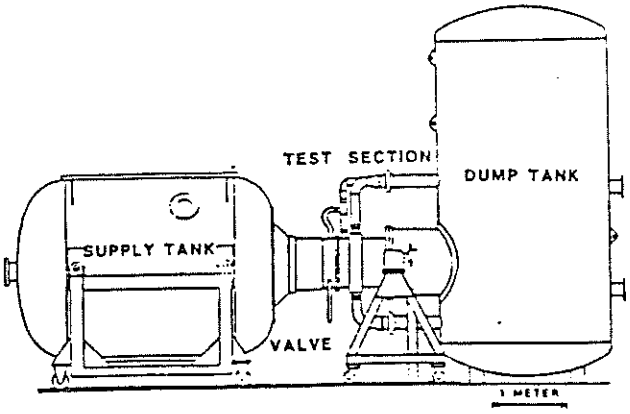

BLOWDOWN TURBINE FACILITY OUTLINE

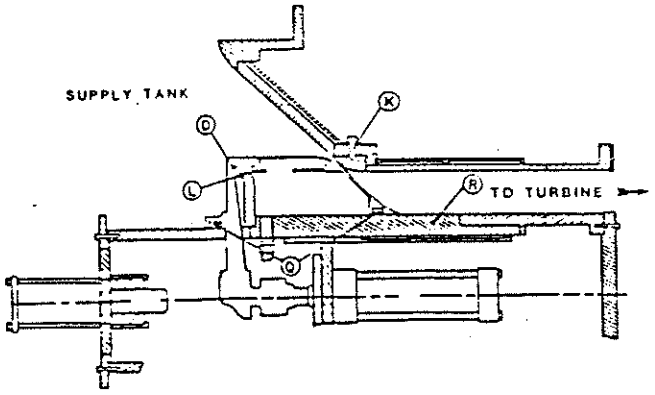

ANNULAR PLUG MAIN FLOW VALVE:
SLIDER (D) DIAMETER IS 0.65 m

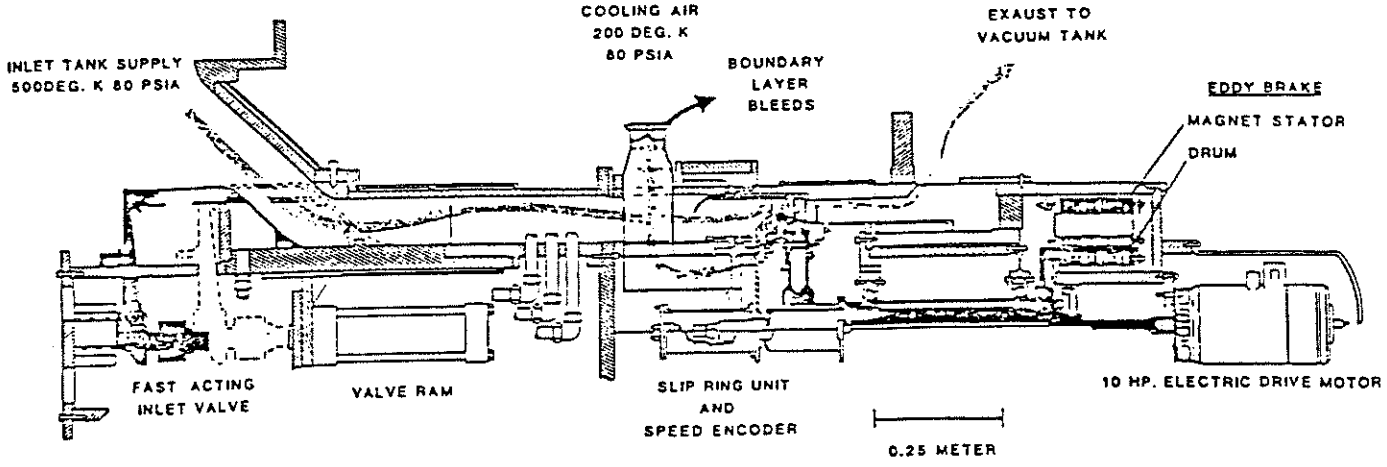

4. BLOWDOWN TURBINE FACILITY DEVELOPED BY EPSTEIN and al. AT MIT (Ref. 24)

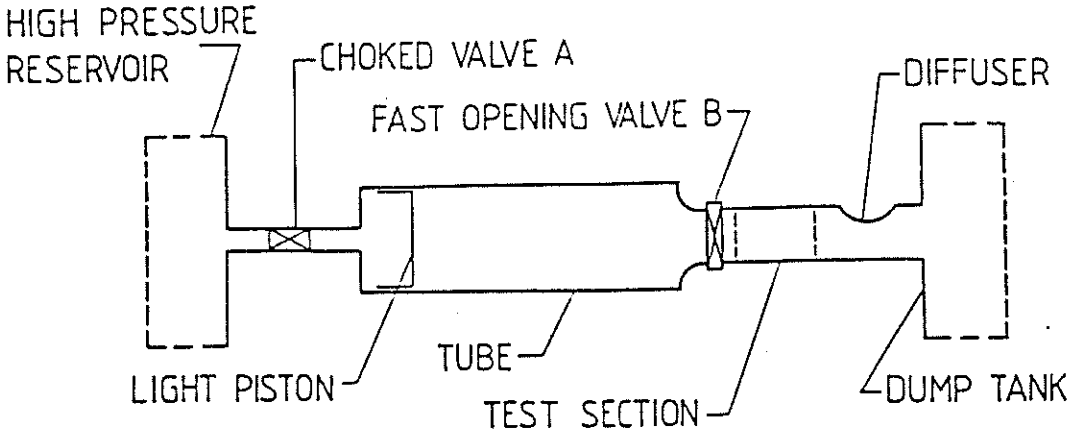

(a)

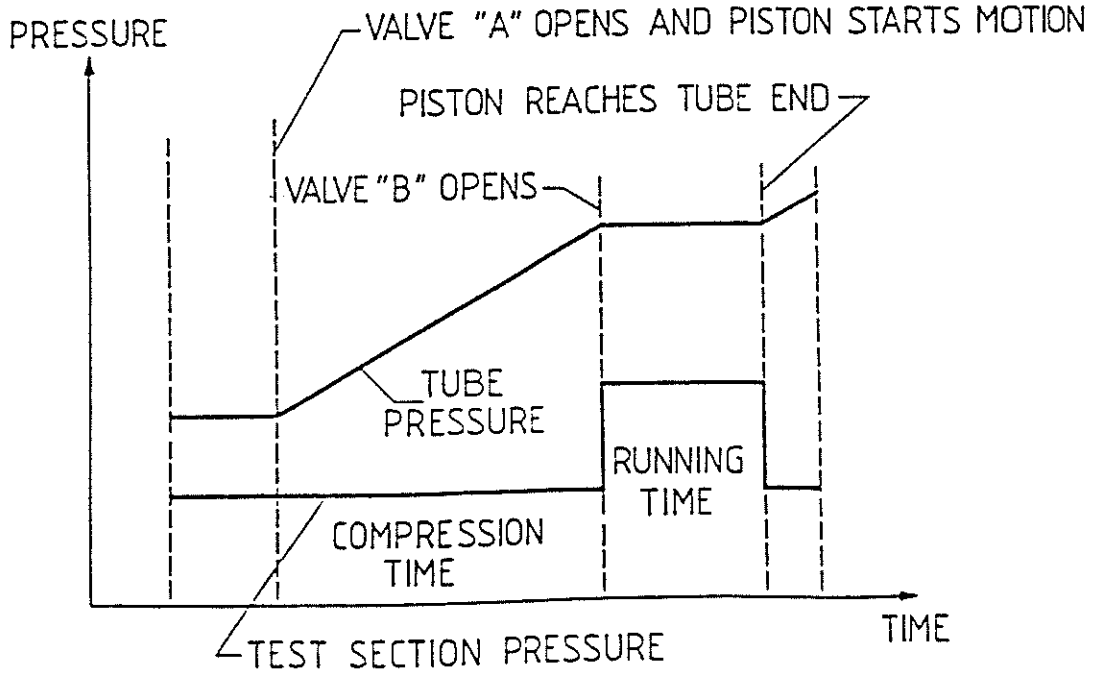

(b)

5. OPERATION PRINCIPLE OF THE ISENTROPIC LIGHT PISTON COMPRESSION TUBE FACILITY

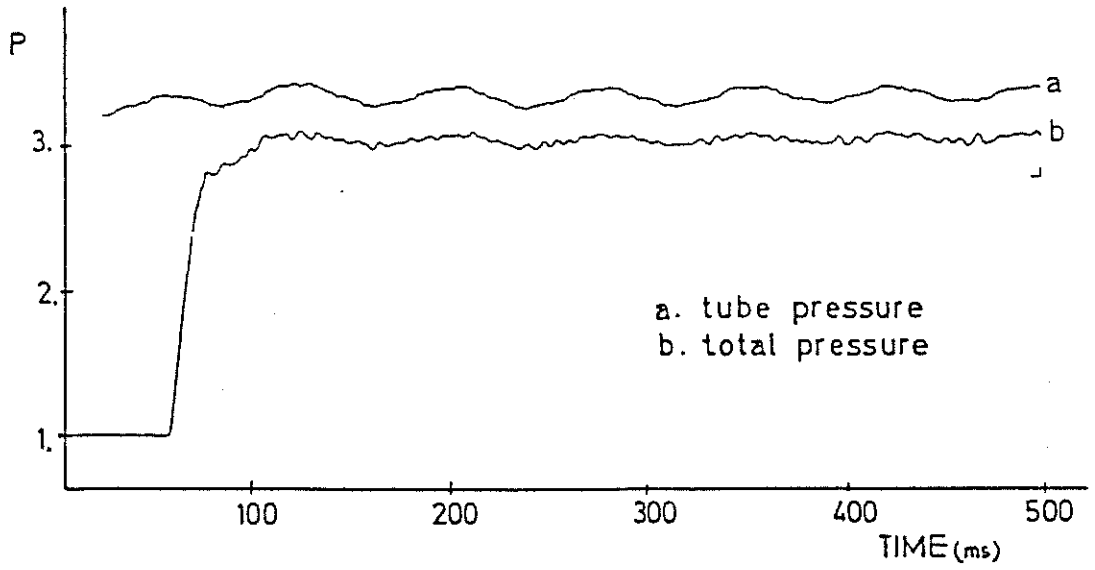

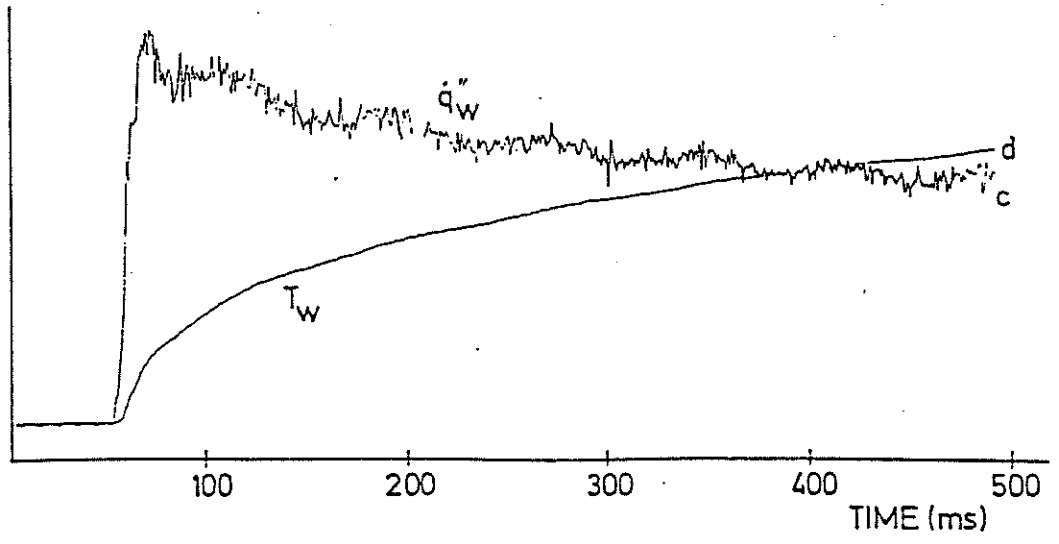

6. EVOLUTION IN TIME OF SOME TYPICAL FLOW VARIABLES MEASURED IN AN ISENTROPIC LIGHT PISTON COMPRESSION TUBE FACILITY

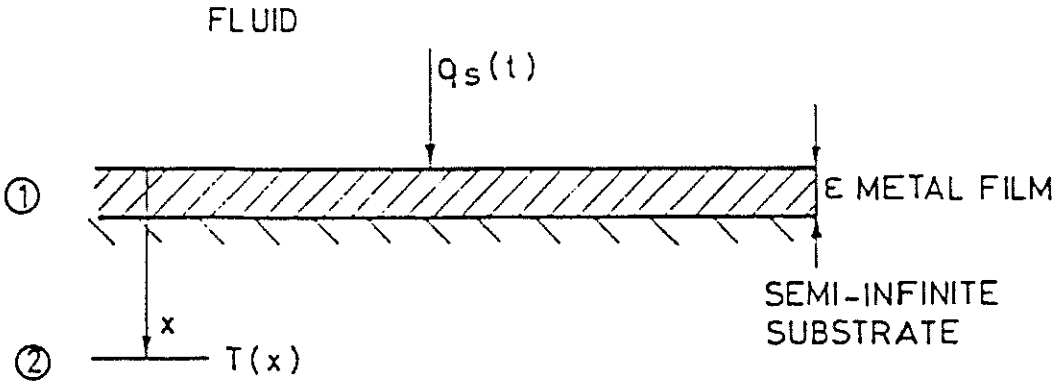

7. TRANSIENT HEAT CONDUCTION IN A SEMI-INFINITE BODY

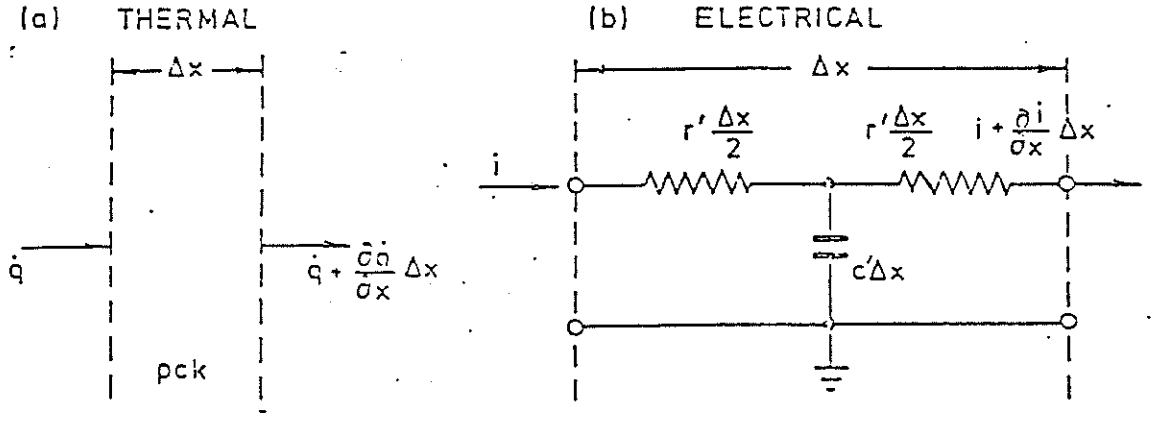

8. ELECTRICAL ANALOGY OF HEAT TRANSFER INTO A SEMI-INFINITE BODY

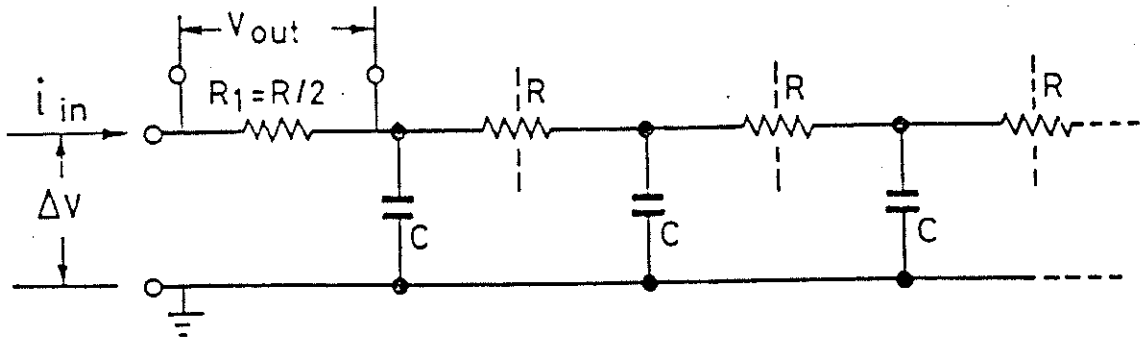

9. ANALOG HEAT TRANSFER CIRCUITS

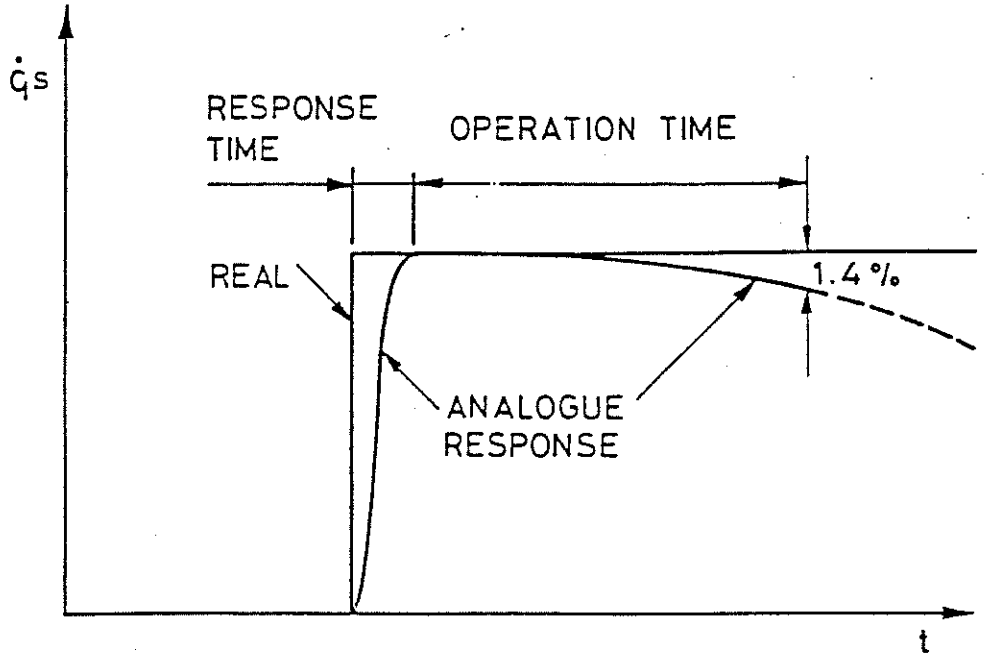

10. CHARACTERISTIC TIMES OF AN ANALOG HEAT TRANSFER CIRCUIT

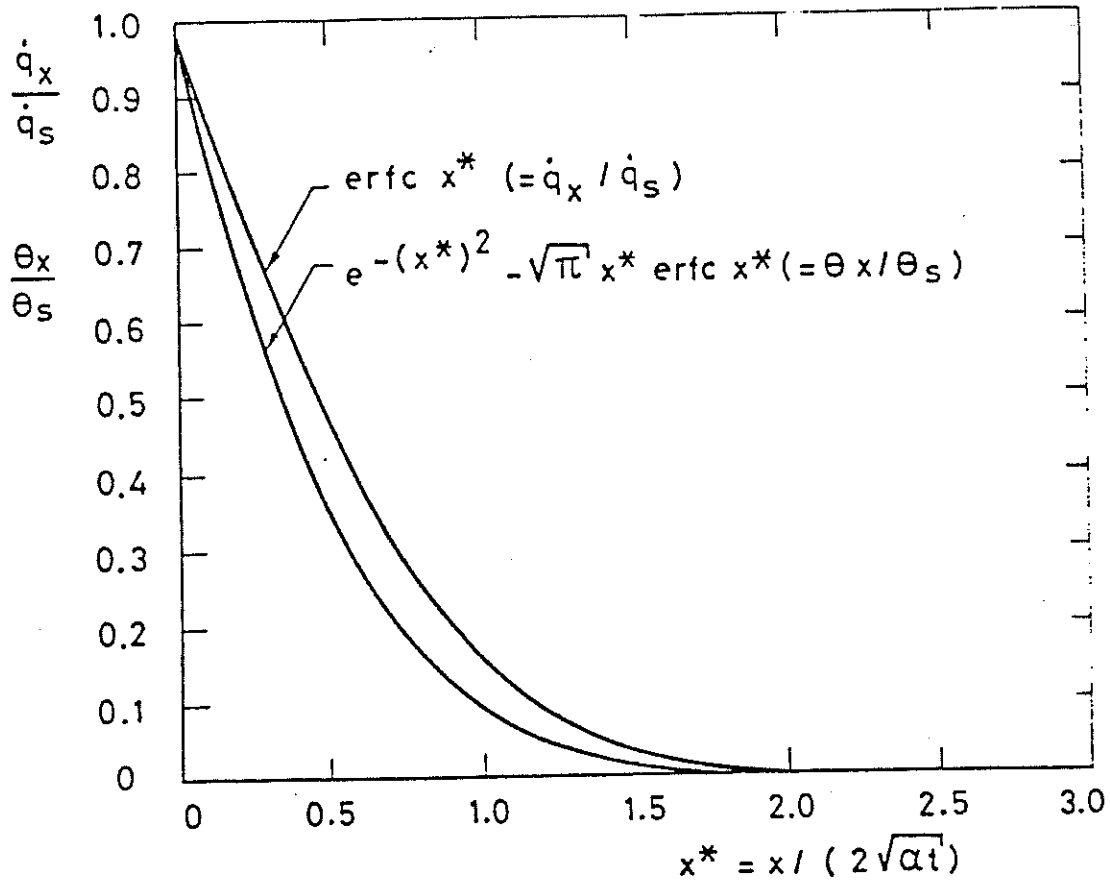

11. PENETRATION OF A THERMAL PULSE INTO A SUBSTRATE AFTER A STEP FUNCTION IN SURFACE HEAT FLUX
(Ref. 29)

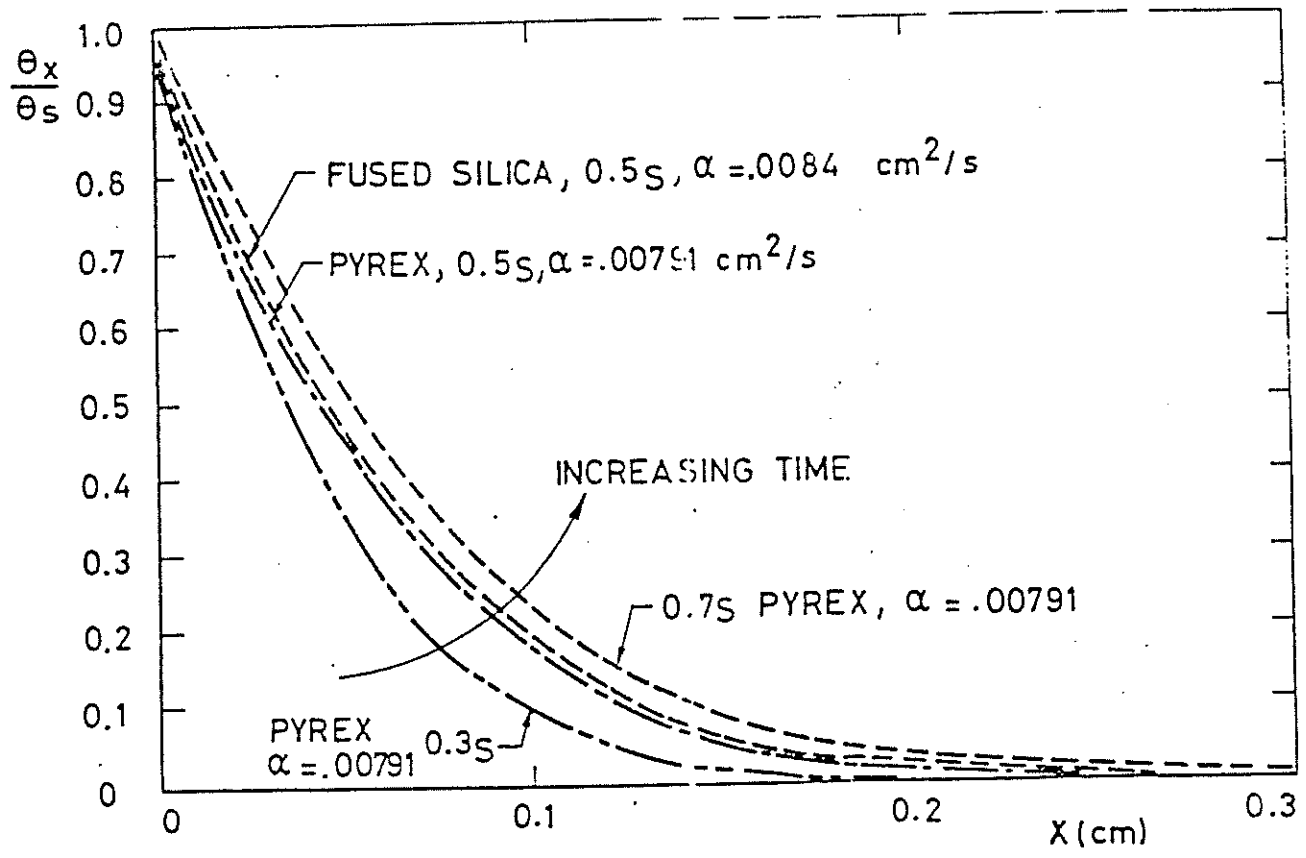

12. PENETRATION OF A THERMAL PULSE INTO A SUBSTRATE AFTER A STEP FUNCTION IN SURFACE HEAT FLUX

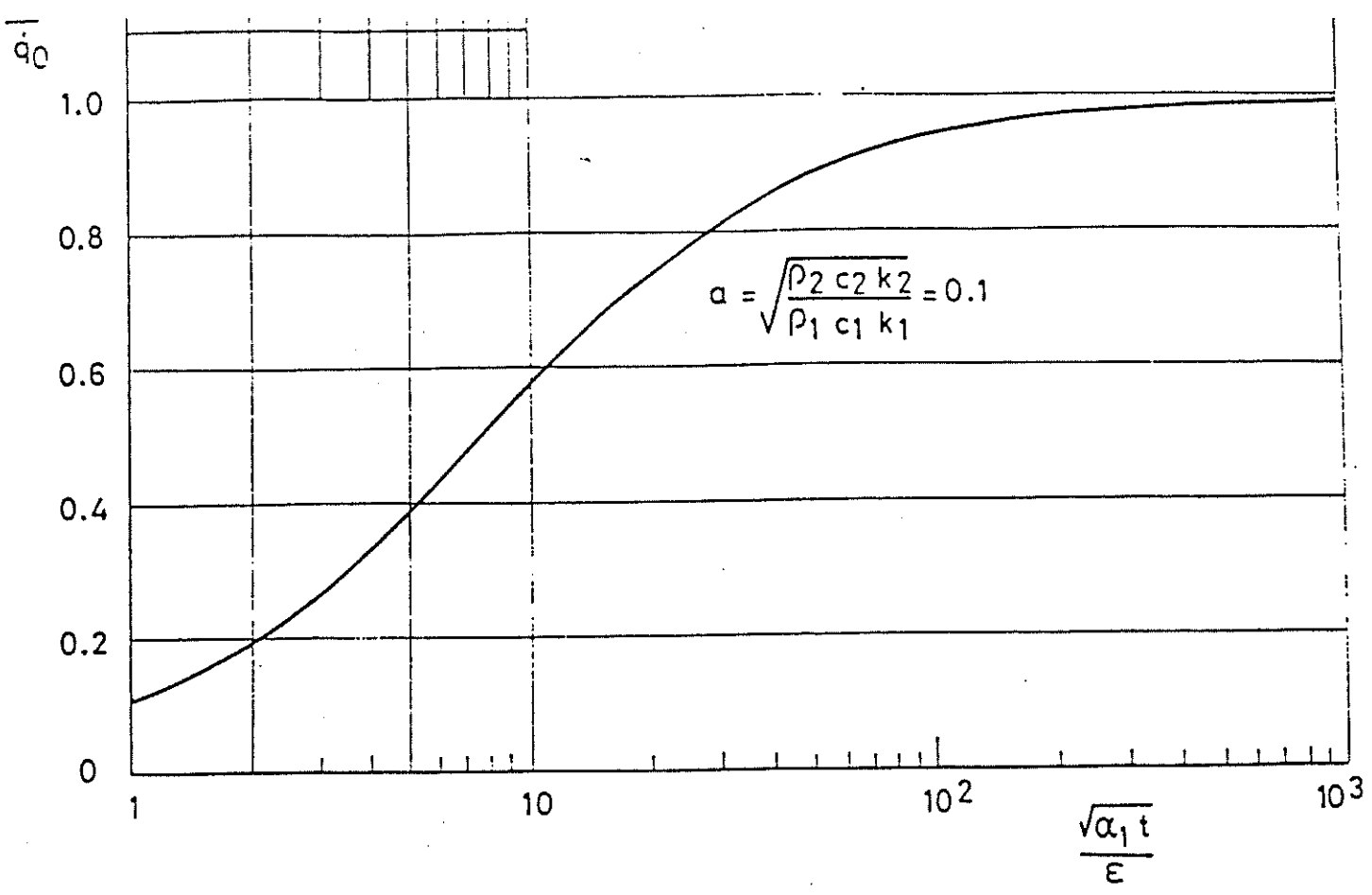

13. THIN FILM GAUGE THICKNESS INFLUENCE

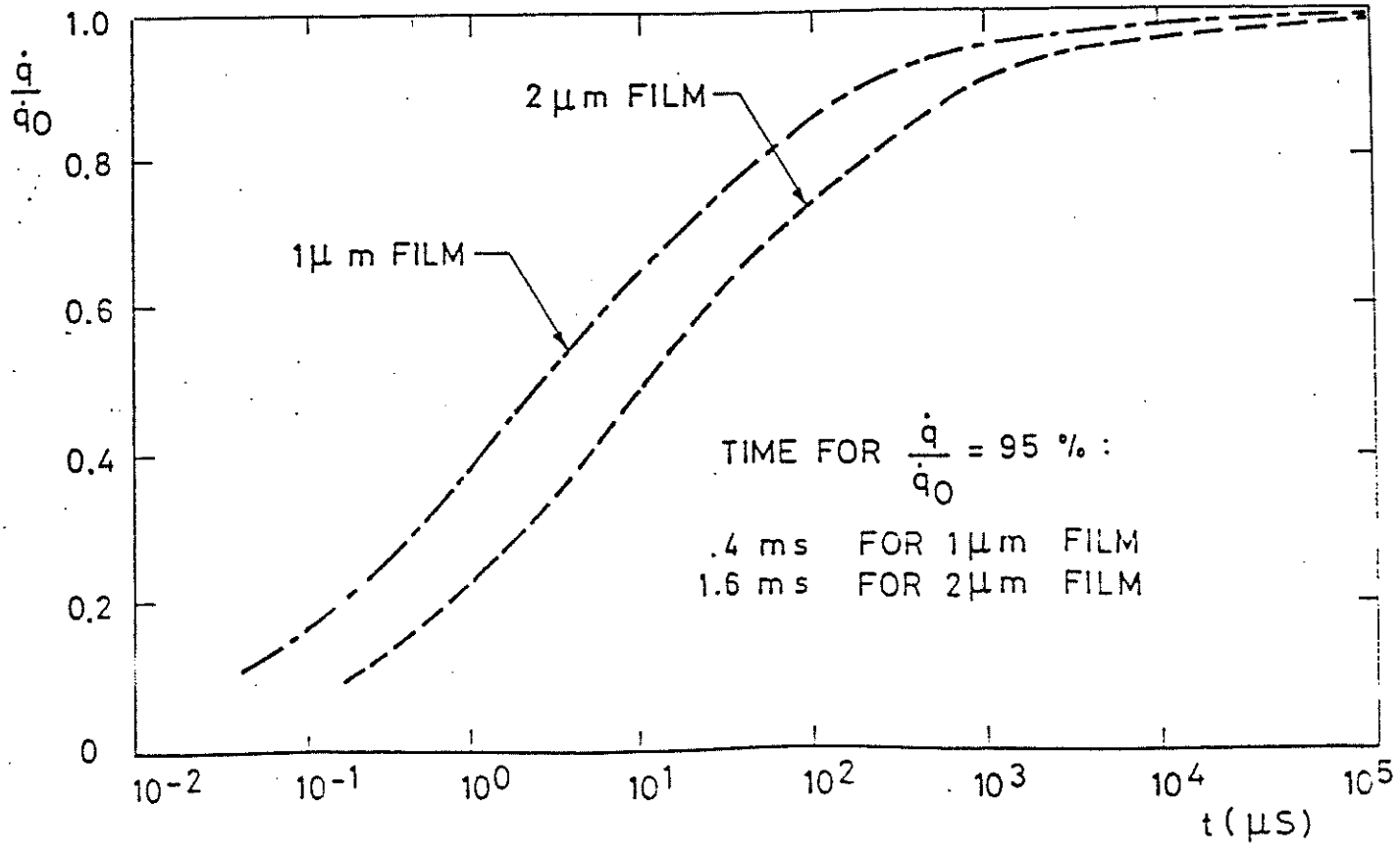

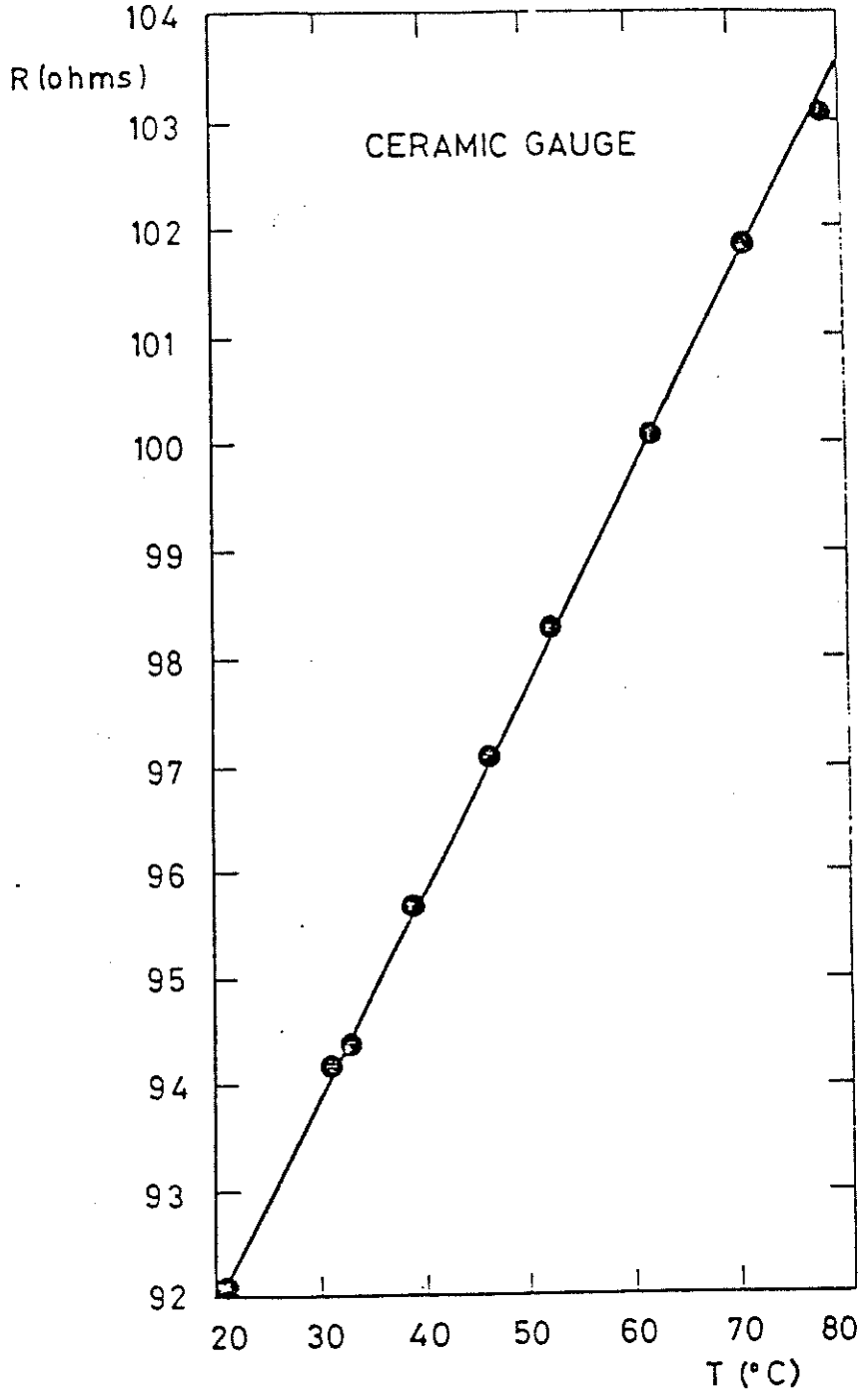

15. TYPICAL ΔR/ΔT CALIBRATION CURVE

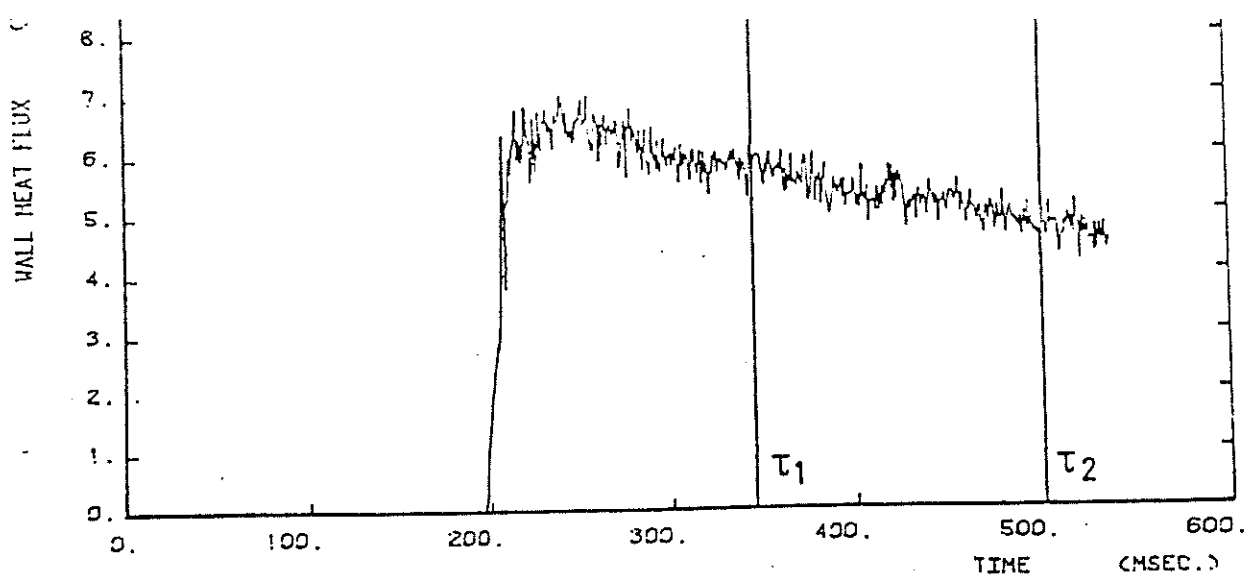
WALL HEAT FLUX
6.
7.
6.
5.
4.
3.
2.
1.
0.
τ_1
τ_2
0.
100.
200.
300.
400.
500.
600.
TIME (MSEC.)

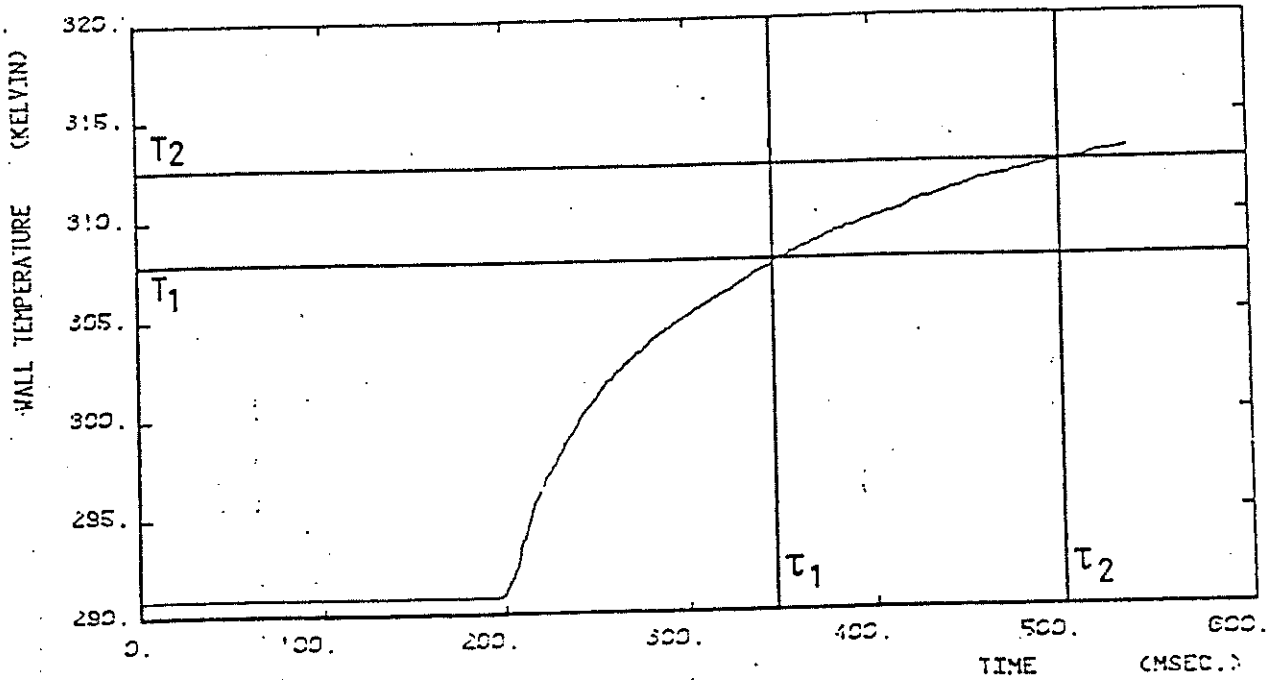
WALL TEMPERATURE (KELVIN)
320.
315.
310.
305.
300.
295.
290.
T_2
T_1
τ_1
τ_2
0.
100.
200.
300.
400.
500.
600.
TIME (MSEC.)

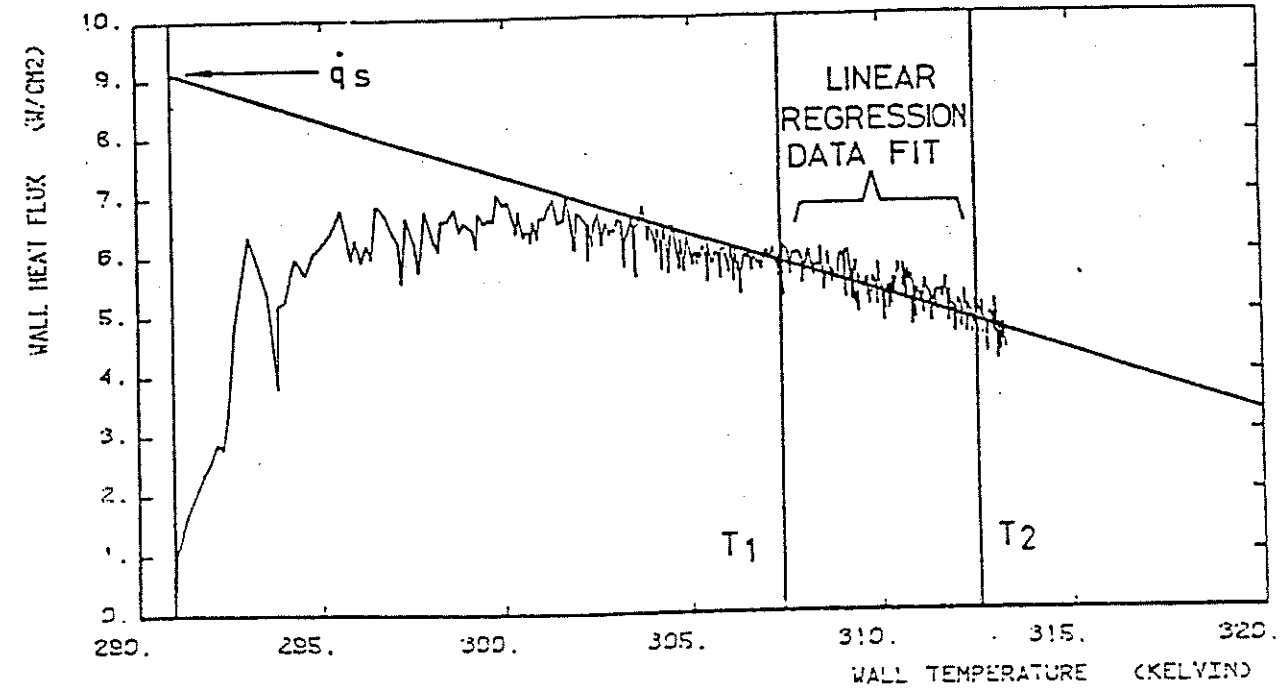
WALL HEAT FLUX (W/CM2)
10.
9.
6.
7.
6.
5.
4.
3.
2.
1.
0.
$\dot{q}_s$
LINEAR
REGRESSION
DATA FIT
T_1
T_2
290.
295.
300.
305.
310.
315.
320.
WALL TEMPERATURE (KELVIN)

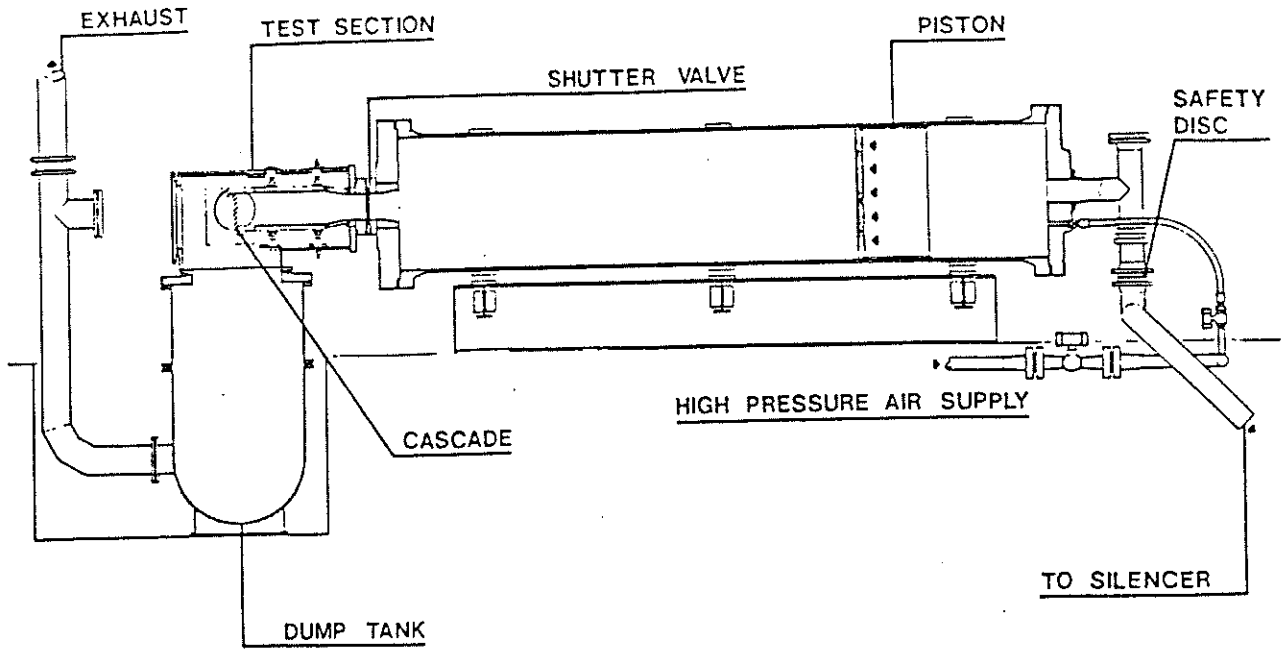

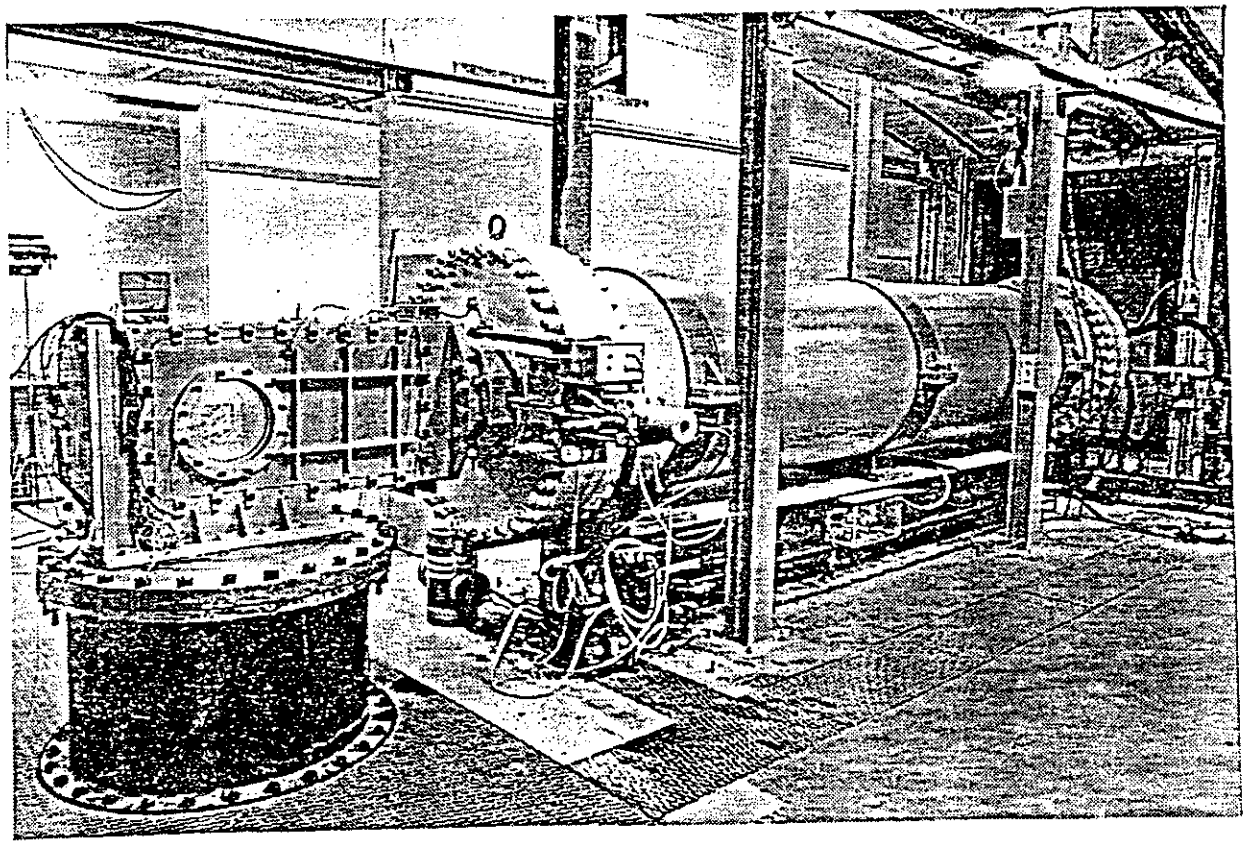

17. VKI ISENTROPIC COMPRESSION TUBE FACILITY

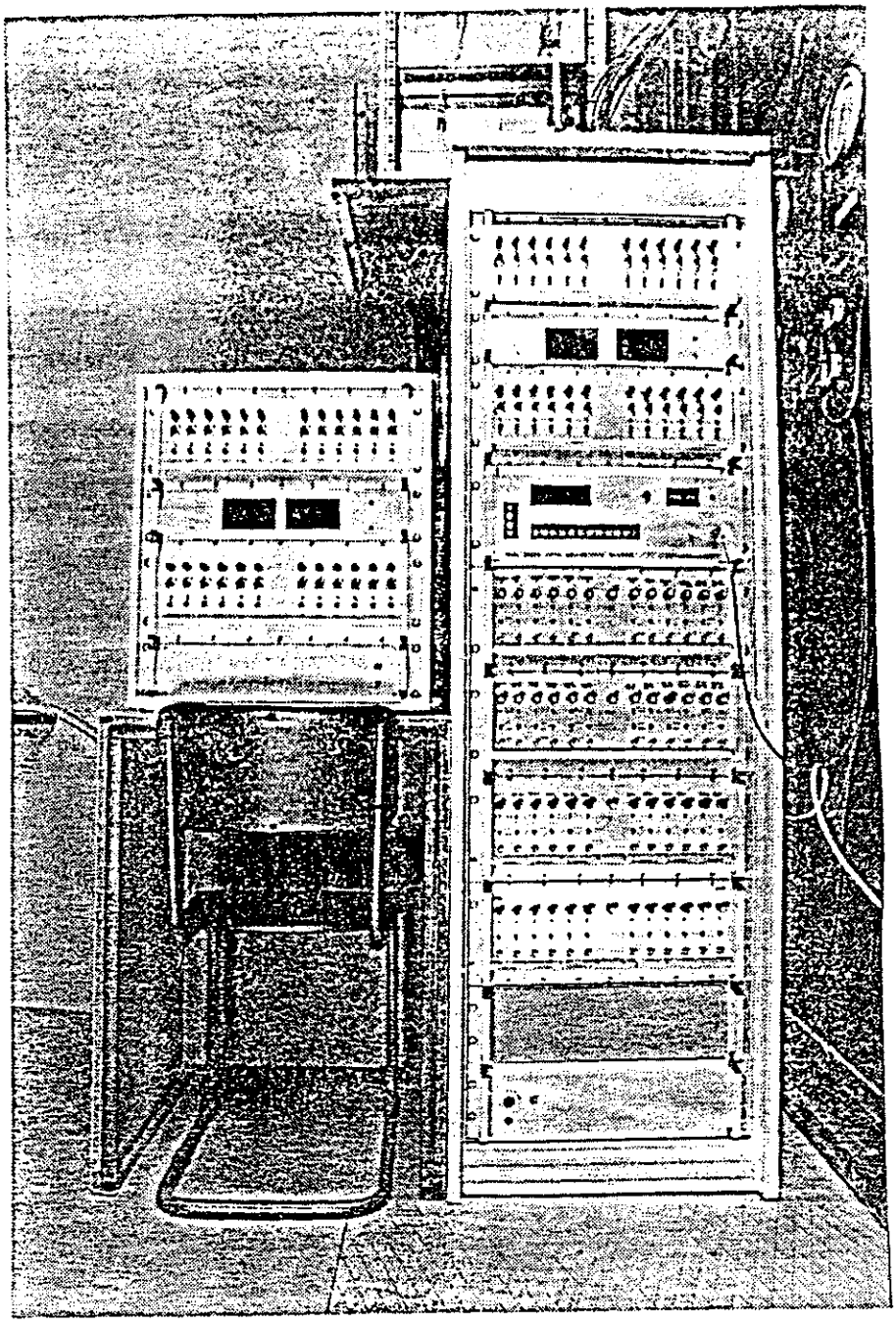

18. VKI HIGH SPEED DATA ACQUISITION SYSTEM

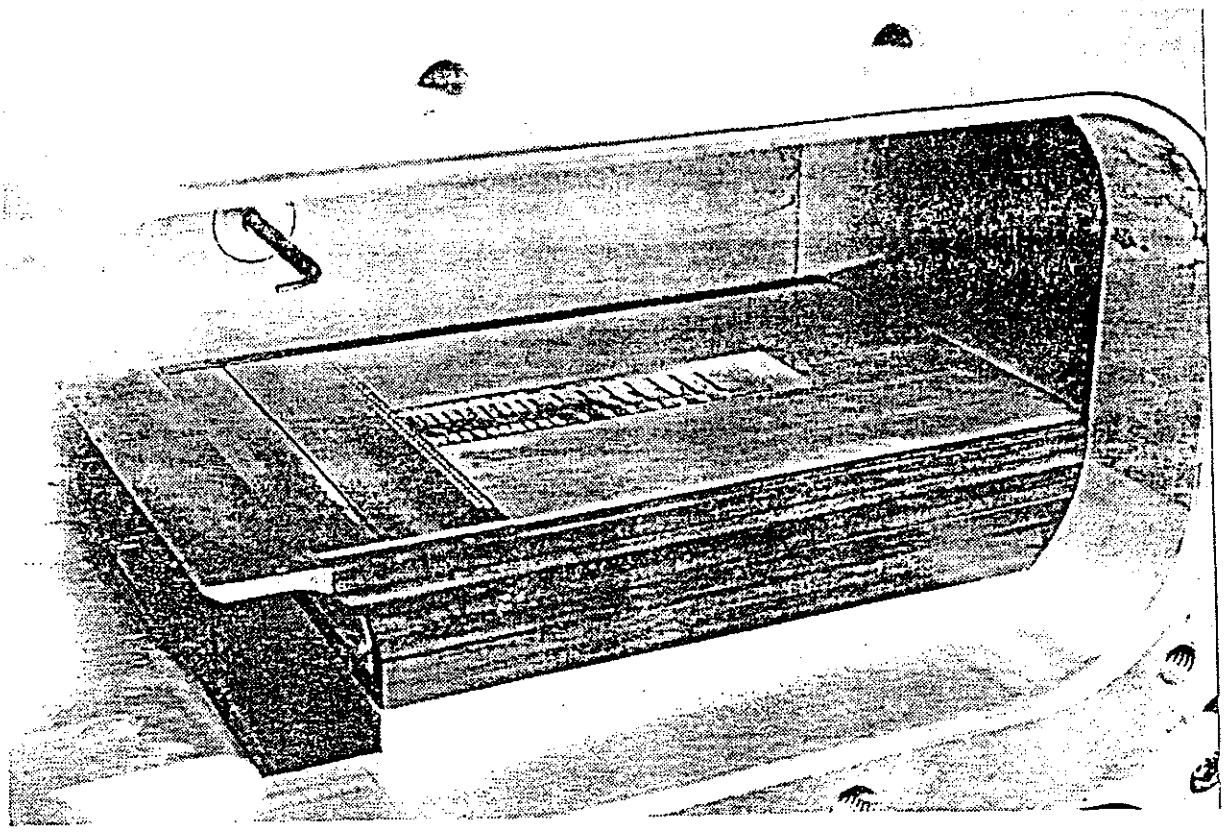

19. FLAT PLATE MODEL

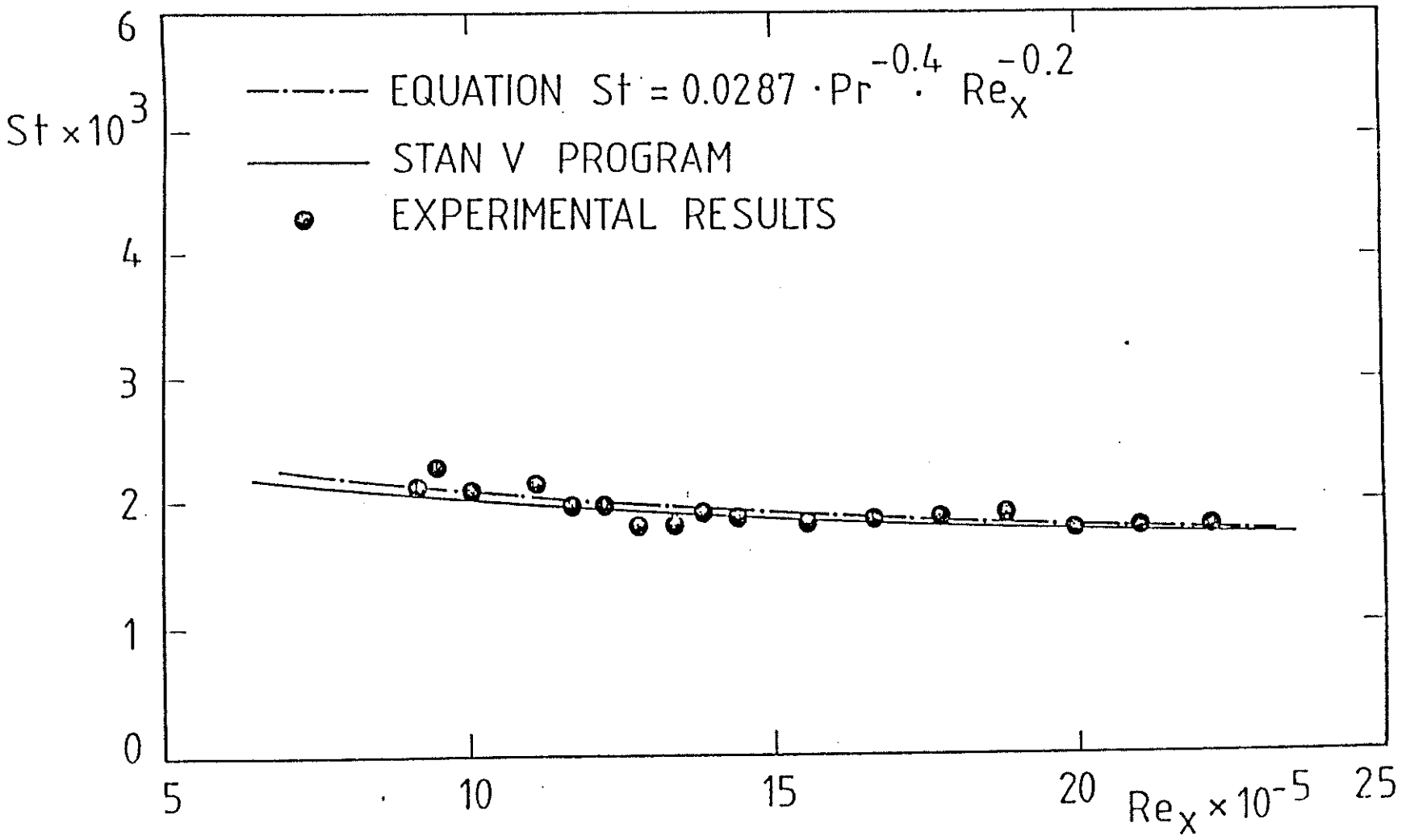

20. FLAT PLATE HEAT TRANSFER WITHOUT FILM COOLING

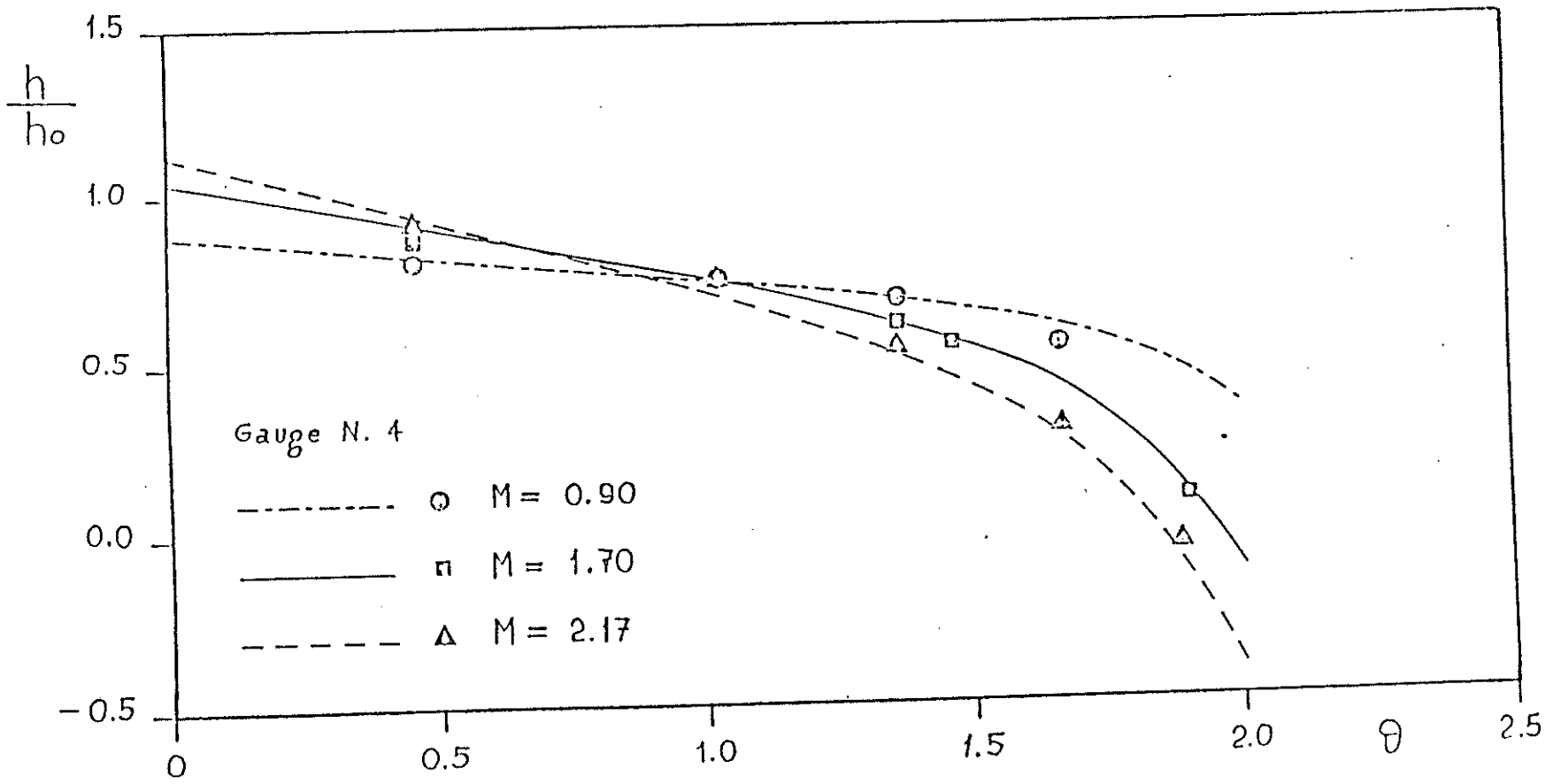

21. FLAT PLATE HEAT TRANSFER WITH FILM COOLING

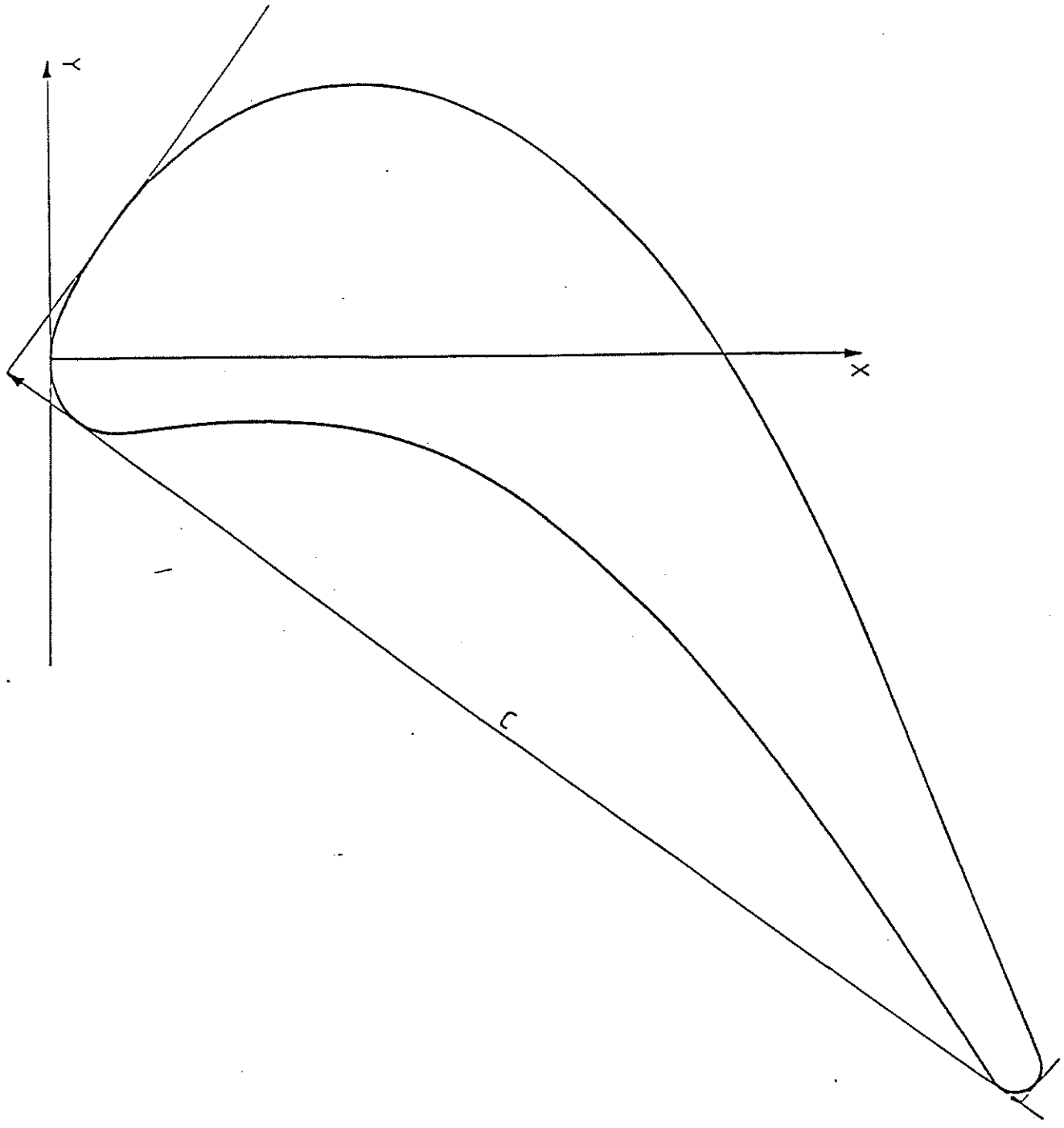

22. HIGH PRESSURE ROTOR BLADE WITHOUT FILM COOLING : MODEL DESCRIPTION

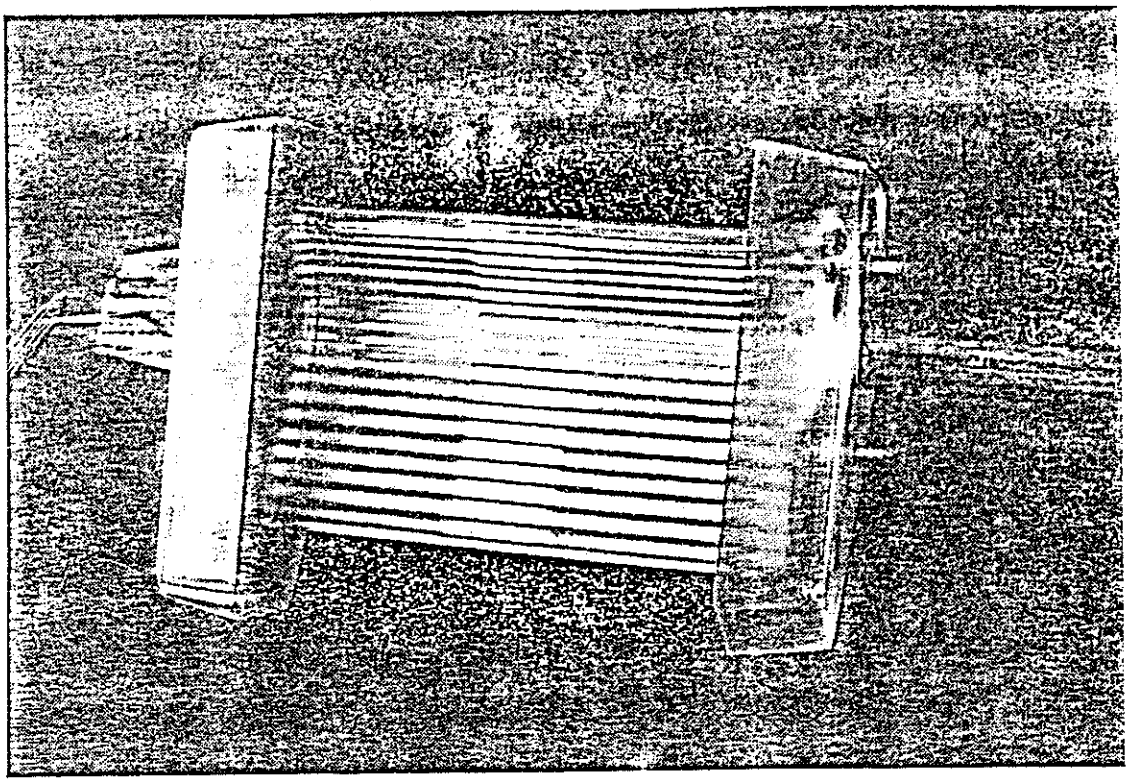

23. HIGH PRESSURE ROTOR BLADE WITHOUT FILM COOLING :
HEAT TRANSFER INSTRUMENTED BLADE

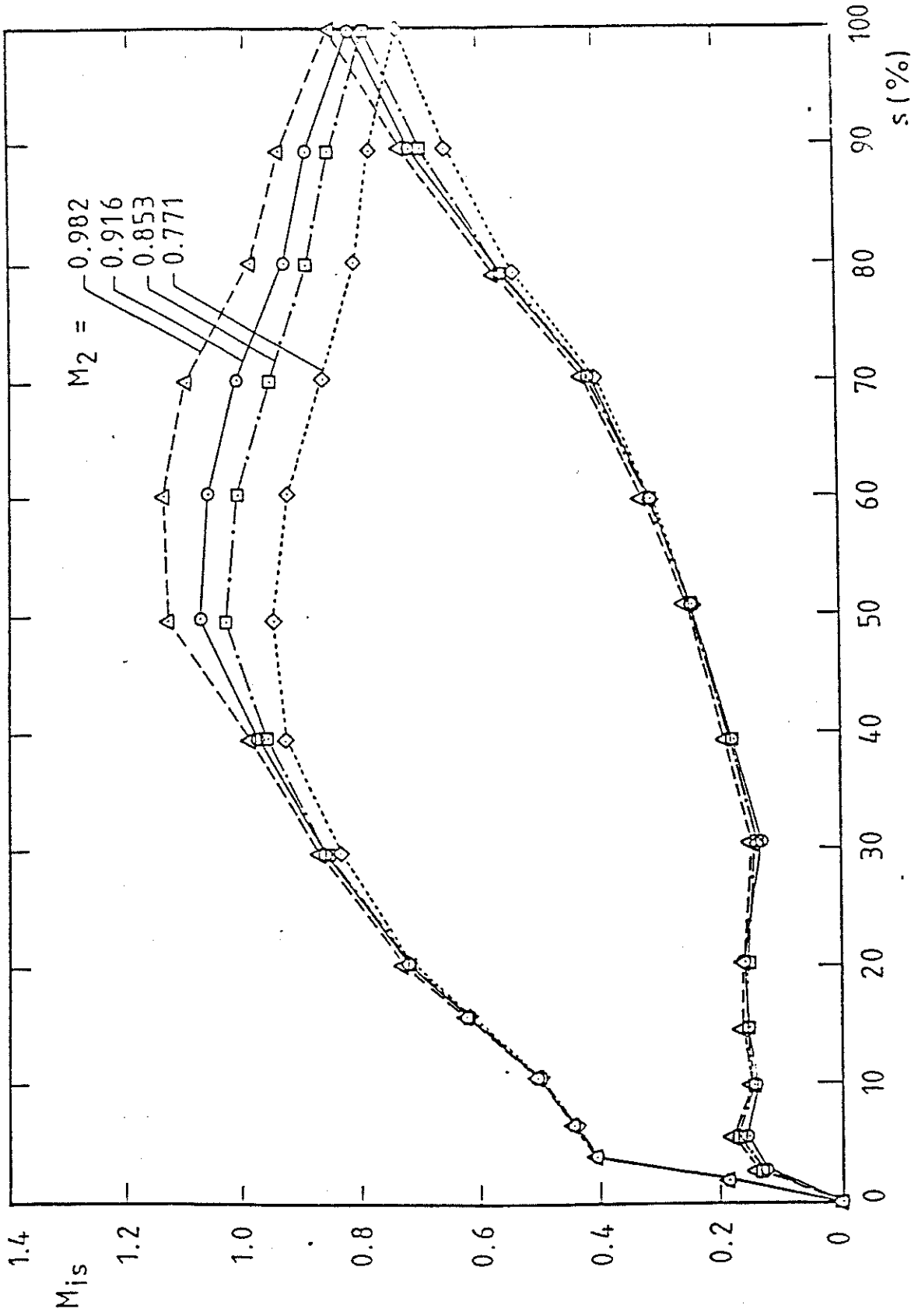

24. HIGH PRESSURE ROTOR BLADE WITHOUT FILM COOLING : VELOCITY DISTRIBUTION

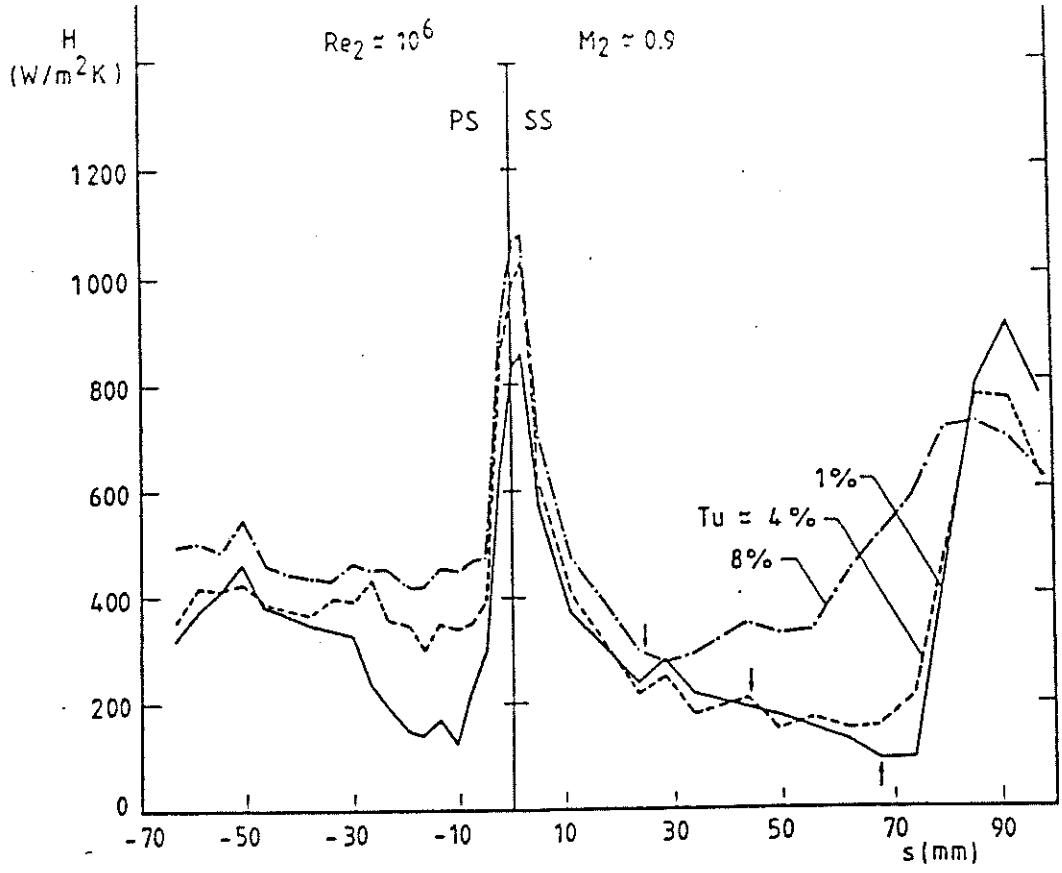

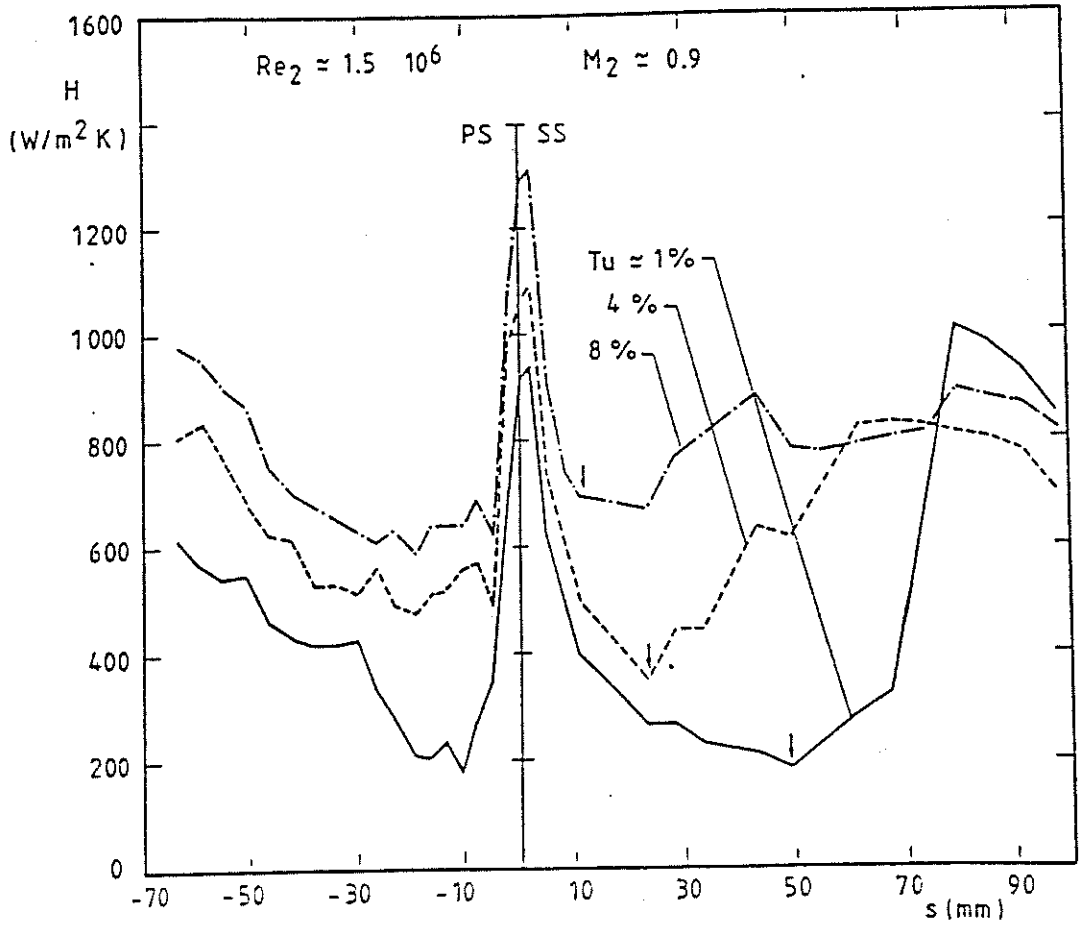

25. HIGH PRESSURE ROTOR BLADE WITHOUT FILM COOLING

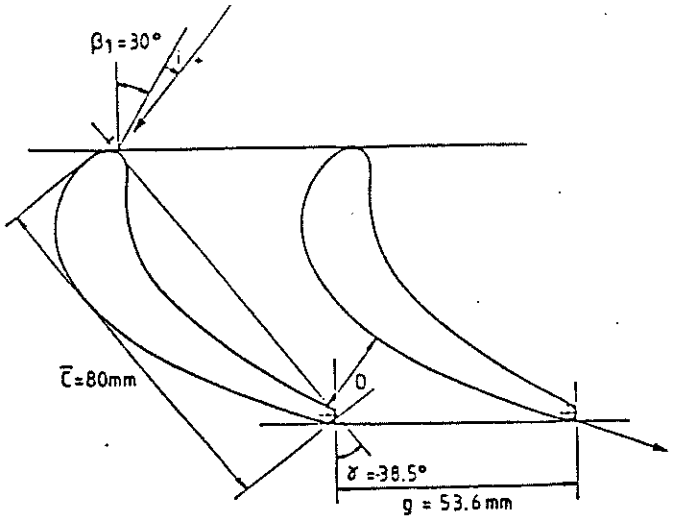

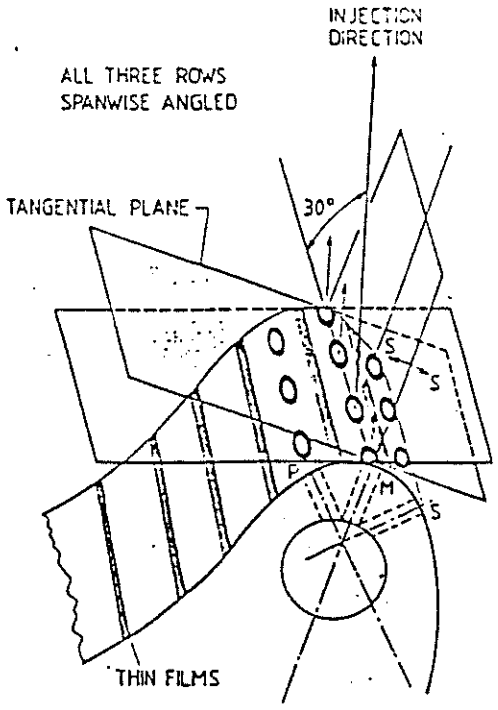

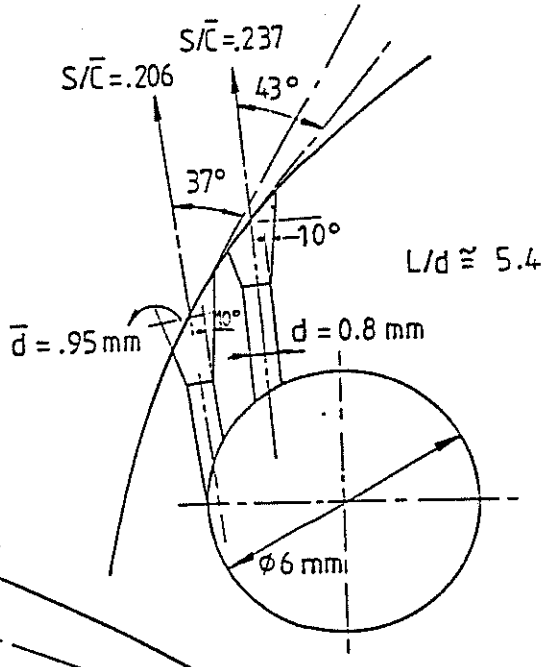

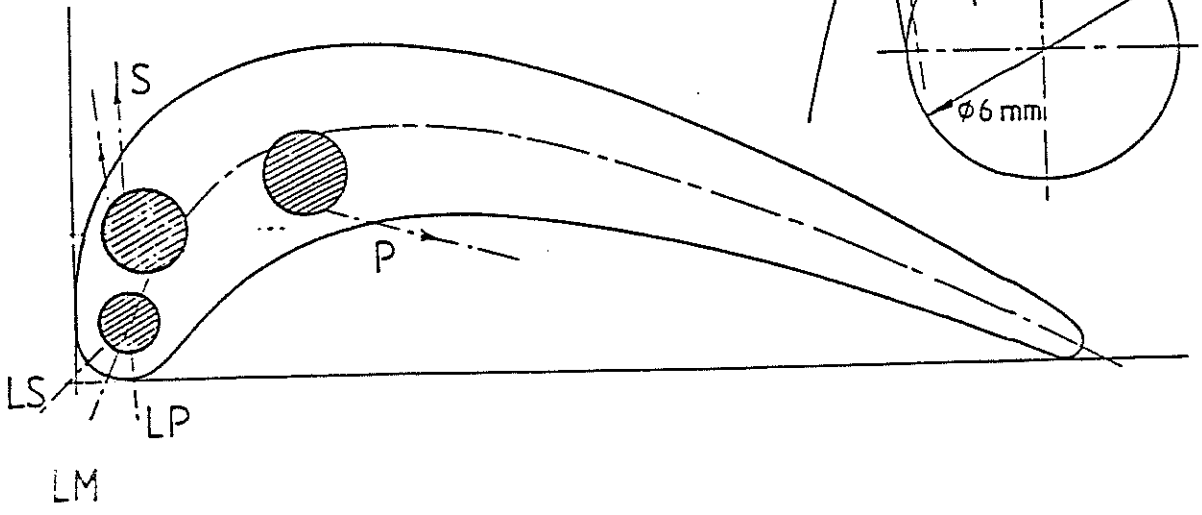

27. HIGH PRESSURE ROTOR BLADE WITH FILM COOLING :

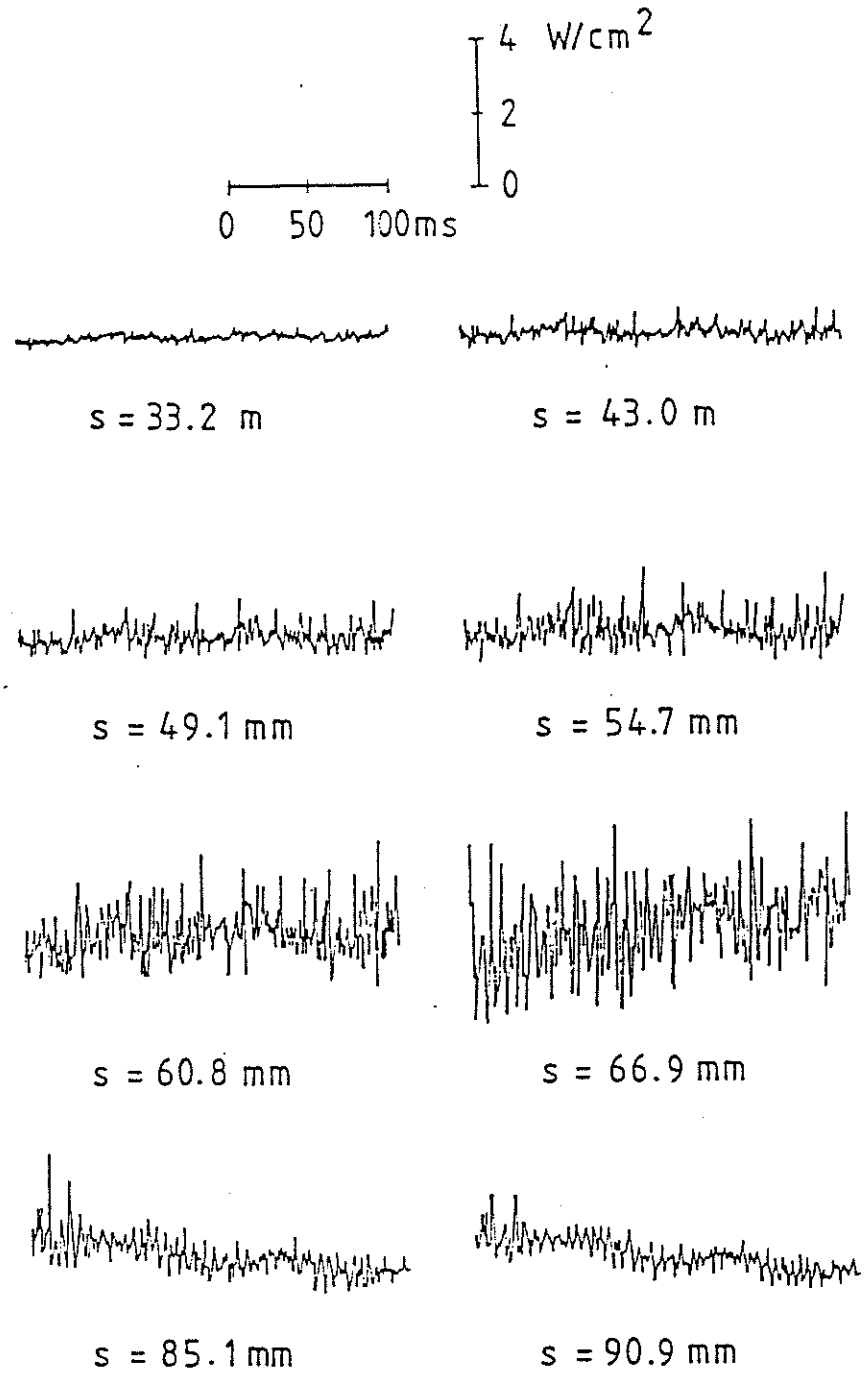

26. HIGH PRESSURE ROTOR BLADE WITHOUT FILM COOLING :
TRANSITION ONSET DETERMINATION ALONG THE SUCTION SIDE

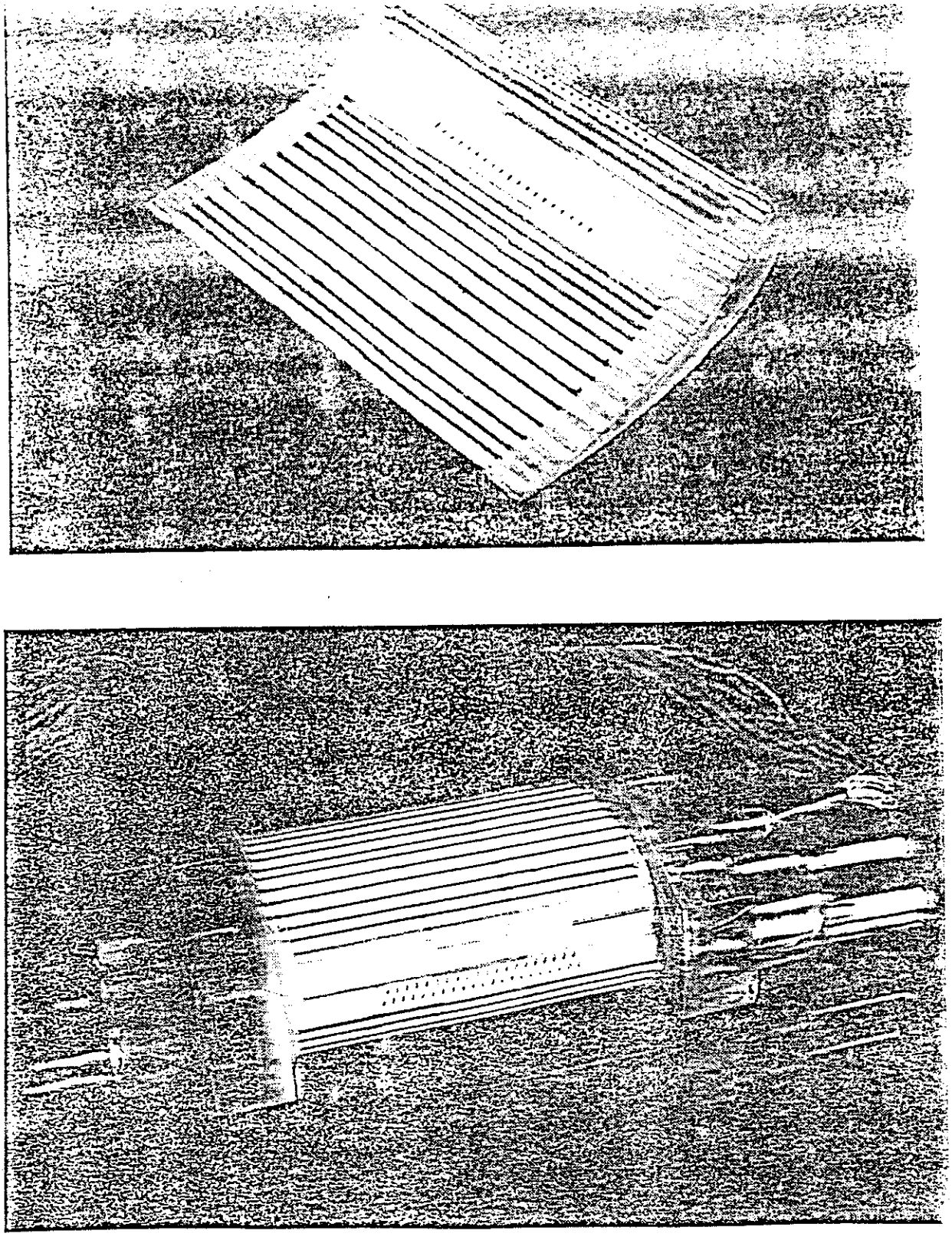

28. HIGH PRESSURE ROTOR BLADE WITH FILM COOLING : HEAT TRANSFER INSTRUMENTED BLADE

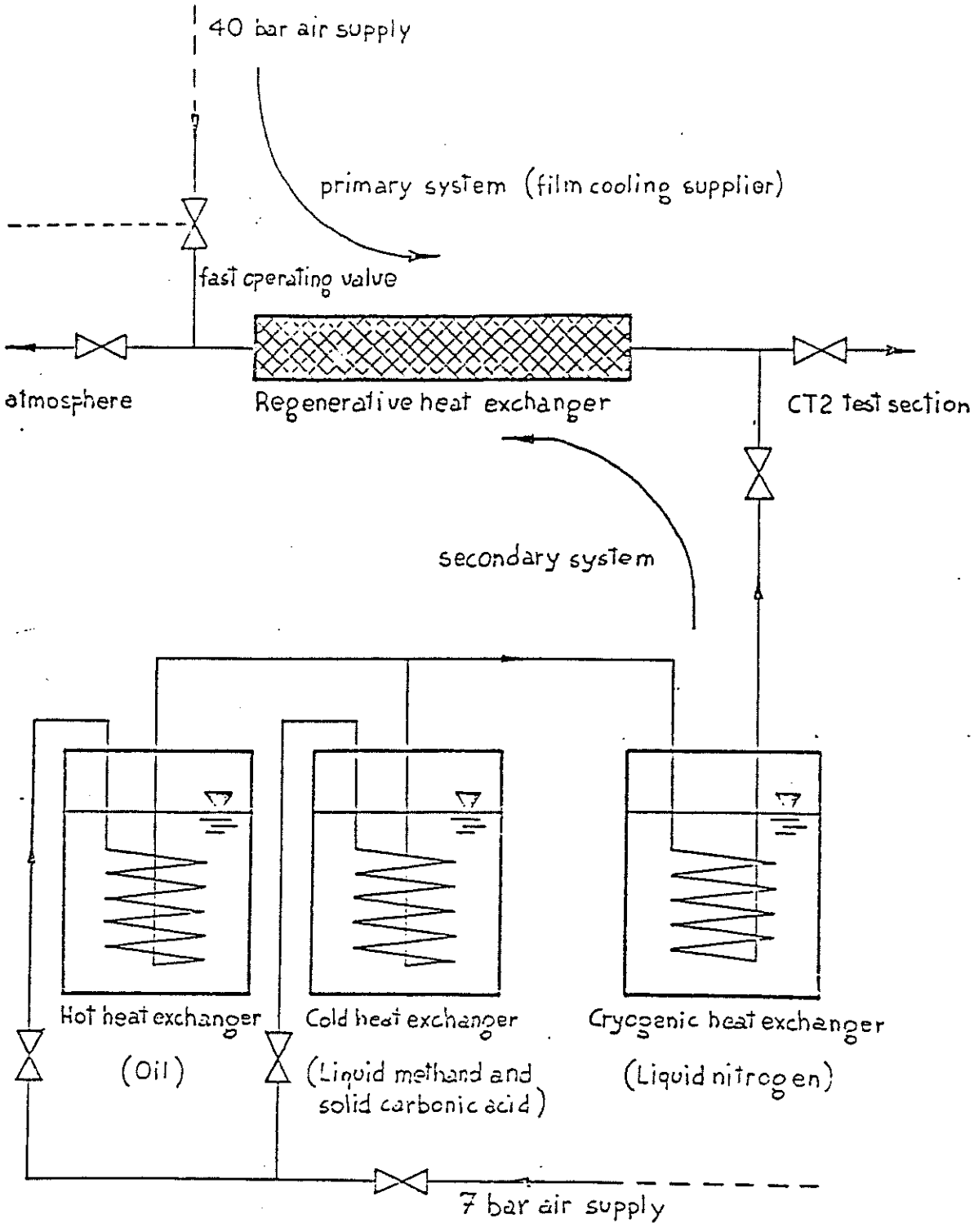

29. COOLANT FLOW PRODUCTION

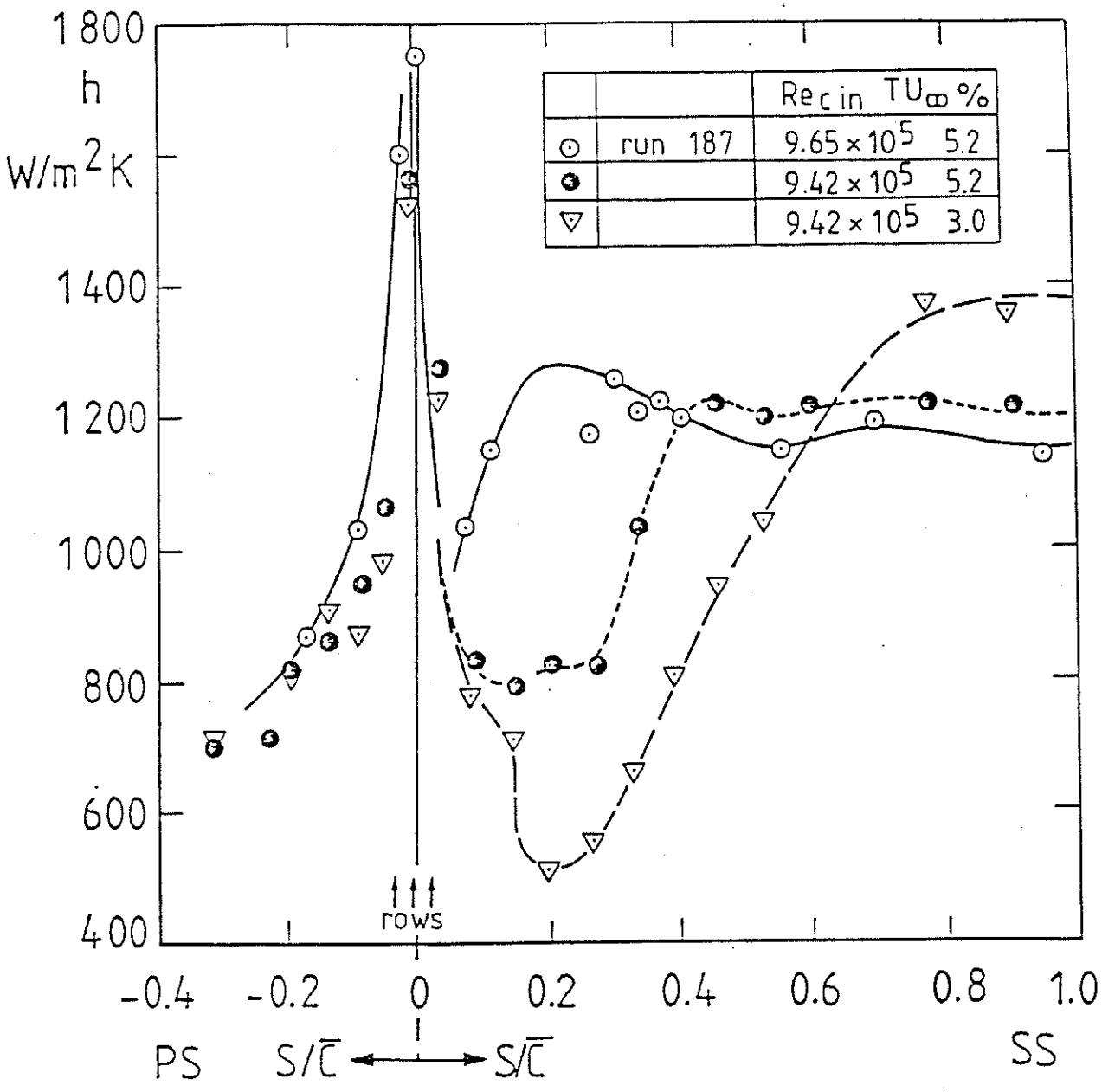

30. HIGH PRESSURE ROTOR BLADE WITH FILM COOLING :
EFFECT OF COOLING HOLES ON BOUNDARY LAYER TRANSITION

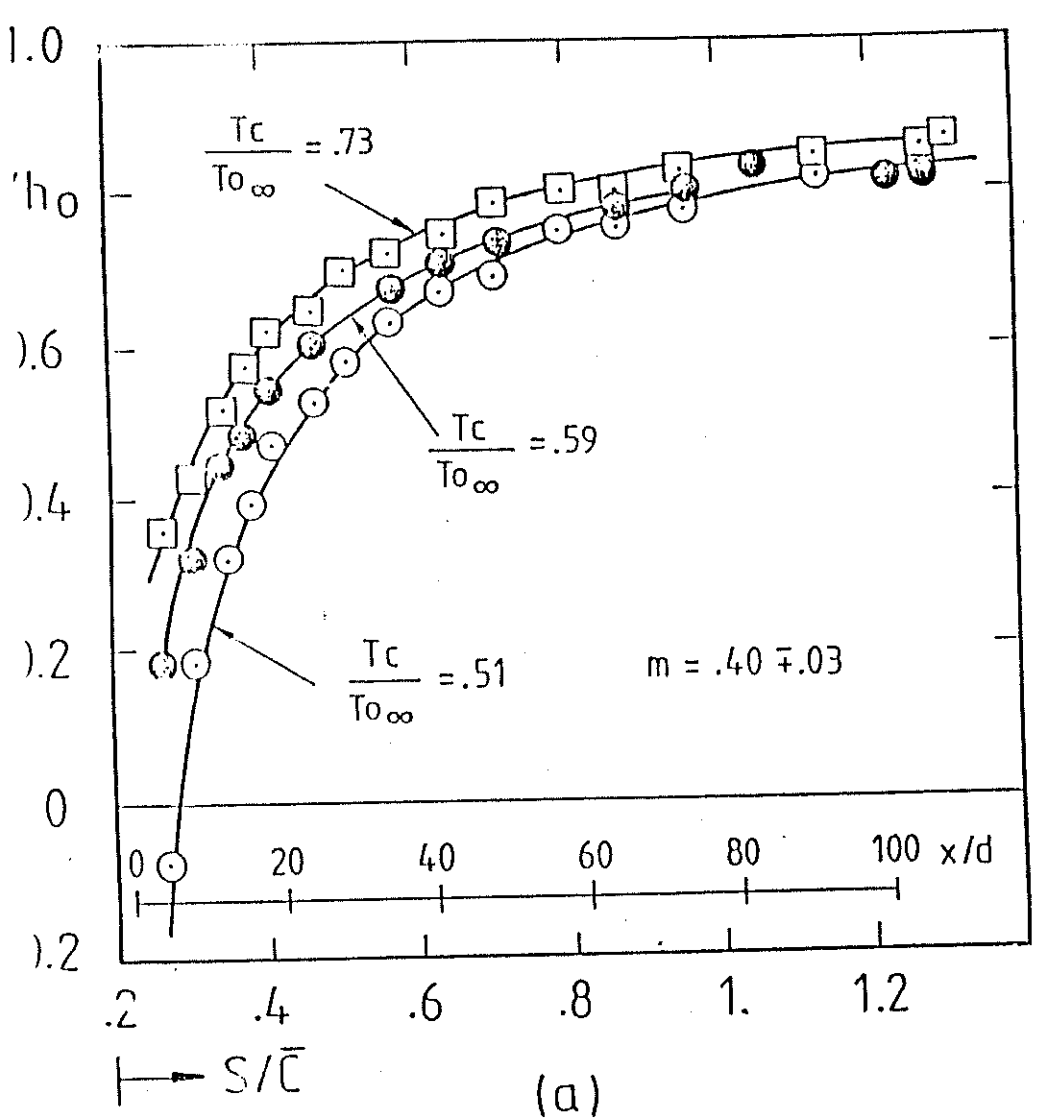

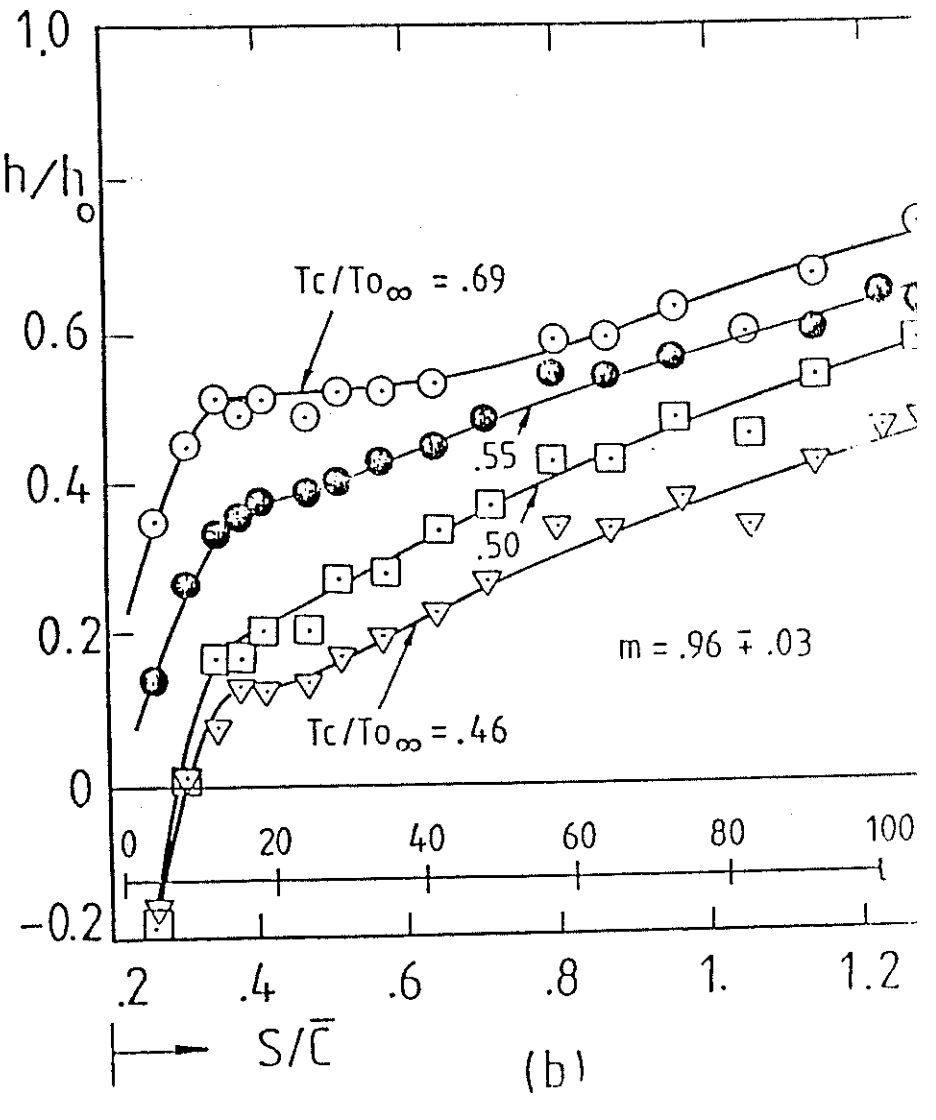

31. HIGH PRESSURE ROTOR BLADE WITH FILM COOLING :
EFFECT OF COOLANT TEMPERATURE ON THE HEAT TRANSFER DISTRIBUTION